Bioactive Materials 24 (2023) 387–400

Contents lists available at ScienceDirect

Bioactive Materials

journal homepage: www.keaipublishing.com/en/journals/bioactive-materials

Mechano-responsive hydrogel for direct stem cell manufacturing to therapy

Yufeng Shou [a,b,1], Ling Liu [b,d,1], Qimin Liu [c,1], Zhicheng Le [a,b], Khang Leng Lee [e], Hua Li [f], Xianlei Li [a,b], Dion Zhanyun Koh [a], Yuwen Wang [a], Tong Ming Liu [g], Zheng Yang [d,h], Chwee Teck Lim [a,b,i], Christine Cheung [e,g], Andy Tay [a,b,d,*]

[a] Department of Biomedical Engineering, National University of Singapore, 117583, Singapore
[b] Institute for Health Innovation & Technology, National University of Singapore, 117599, Singapore
[c] School of Civil Engineering and Architecture, Wuhan University of Technology, 430070, Wuhan, China
[d] NUS Tissue Engineering Program, National University of Singapore, 117510, Singapore
[e] Lee Kong Chian School of Medicine, Nanyang Technological University, 636921, Singapore
[f] School of Mechanical and Aerospace Engineering, Nanyang Technological University, 639798, Singapore
[g] Institute of Molecular and Cell Biology, Agency for Science, Technology and Research (A*STAR), 138648, Singapore
[h] Department of Orthopaedic Surgery, Yong Loo Lin School of Medicine, National University of Singapore, 119288, Singapore
[i] Mechanobiology Institute, National University of Singapore, 117411, Singapore

ARTICLE INFO

Keywords:
Mesenchymal stem cell
Dynamic mechanical stimulation
Magnetic hydrogel
Stem cell manufacturing
Cell therapy

ABSTRACT

Bone marrow-derived mesenchymal stem cell (MSC) is one of the most actively studied cell types due to its regenerative potential and immunomodulatory properties. Conventional cell expansion methods using 2D tissue culture plates and 2.5D microcarriers in bioreactors can generate large cell numbers, but they compromise stem cell potency and lack mechanical preconditioning to prepare MSC for physiological loading expected *in vivo*. To overcome these challenges, in this work, we describe a 3D dynamic hydrogel using magneto-stimulation for direct MSC manufacturing to therapy. With our technology, we found that dynamic mechanical stimulation (DMS) enhanced matrix-integrin β1 interactions which induced MSCs spreading and proliferation. In addition, DMS could modulate MSC biofunctions including directing MSC differentiation into specific lineages and boosting paracrine activities (e.g., growth factor secretion) through YAP nuclear localization and *FAK-ERK* pathway. With our magnetic hydrogel, complex procedures from MSC manufacturing to final clinical use, can be integrated into one single platform, and we believe this 'all-in-one' technology could offer a paradigm shift to existing standards in MSC therapy.

1. Introduction

Bone marrow-derived mesenchymal stem cells (MSCs) are multipotent stem cells found in bone tissues that play key roles in tissue regeneration and immuno-modulation. With specific biochemical and mechanical stimuli, MSCs can proliferate and differentiate into various mesenchymal/mesodermal cell lineages. Their secretome can also induce paracrine signalling, and when coupled with self-renewal and differentiation, make MSC as a powerful tool for regenerative medicine [1–5]. As of September 2022, there are over 1400 registered clinical trials worldwide listed on ClinicalTrials.gov using MSCs to investigate the therapeutic effect, of which up to 67% were in phase I or II [6,7].

To fully realize the therapeutic potential of MSCs, significant challenges in MSC manufacturing and delivery/therapy must be overcome: **(1)** Scalable cell expansion while maintaining stemness or controlling differentiation. As an example, current MSC therapy has a recommended dosage of 0.4–9 million cells/kg of recipient body weight for optimal cartilage repair [8,9]. Conventional methods using 2D tissue culture plates or bioreactors with 2.5D microcarriers can achieve ideal cell expansion rate, but these culturing platforms reduce stem cell potency which cause inconsistent therapeutic effectiveness [10]. While culturing MSCs in 3D biomaterials such as hydrogels is less scalable, this helps to

Abbreviations: MSC, Mesenchymal Stem Cell; DMS, Dynamic Mechanical Stimulation; MP, Magnetic Particle.

Peer review under responsibility of KeAi Communications Co., Ltd.

* Corresponding author. Department of Biomedical Engineering, National University of Singapore, 117583, Singapore.
E-mail address: bietkpa@nus.edu.sg (A. Tay).

[1] Co-first author.

https://doi.org/10.1016/j.bioactmat.2022.12.019
Received 9 October 2022; Received in revised form 5 December 2022; Accepted 20 December 2022

reduce cellular senescence, increase cell-matrix interaction, and improve MSC self-renewal and differentiation potential [10–14]. To the best of our knowledge, biomaterial-based MSC manufacturing has been limited to academic interests; **(2)** Mechanical pre-conditioning. Dynamic mechanical pre-conditioning is important to ensure that the stem cells can maintain normal cell functions and withstand static/dynamic loading expected *in vivo* [15,16]. In fact, the U.S. Food and Drug Administration (FDA) guidance specifically calls for inclusion of mechanical pre-conditioning and testing of cell products designed for applications such as cartilage and bone regeneration which constitute ~18% of existing clinical trials using MSCs [17]. However, there are limited techniques that can achieve mechanical pre-conditioning during MSC manufacturing; **(3)** Cell viability and biofunction after delivery. During conventional intravenous injection of MSCs, shear stress in the syringe can significantly reduce cell viability [18]. Furthermore, when MSCs are introduced into the body such as at injury sites, the harsh microenvironment has been shown to adversely affect cell viability. Interestingly, evidence is emerging that the immune response to dead MSCs contributes to therapeutic efficacy [19–22]. Unfortunately, with conventional systemic injection of cells, it is not possible to control and optimize for the best ratio of live to dead MSCs which is key to exploiting the immune system for tissue regeneration [23]. Out of existing manufacturing methods, only the 3D biomaterial system can improve MSC delivery [18].

MSCs are typically expanded using tissue culture plates or microcarriers before intravenous administration or delivery with biomaterials. This is despite the advantage that expanding MSCs in 3D multi-functional biomaterials can significantly improve stemness [24], offer controllable differentiation [25,26], and even enhance MSC cryopreservation and delivery [27]. The reasons for low uptake are scalability and regulatory hurdles. MSCs expand slower in 3D biomaterials than tissue culture plate and microcarriers, and cell number is an important metric for manufacturers. Manufacturers might also be concerned about regulatory hurdles as biomaterials require multiple ingredients and synthesis steps.

One potential way to improve MSC expansion in 3D biomaterials is the use of dynamic mechanical stimulation (DMS) which has been found to regulate and promote MSC biofunctions *in vivo* [28–30]. MSCs can sense mechanical signals from their microenvironment through cell surface receptors like integrins and then transduced the signals to cytoskeleton and nucleus, to accelerate proliferation, and boost growth factor production [30–37]. These studies suggest the potential of controlled DMS to enhance MSC biofunctions which motivate us to create an integrated 3D biomaterial-based platform for MSC manufacturing and therapy.

In this study, we describe a 3D magnetic hydrogel composed of magnetic particles (MPs) embedded in biocompatible gelatin scaffold that we named GPM (Gelatin methacryloyl/Poly (ethylene glycol) diacrylate-Magnetic particle) hydrogel. The advantage of using MPs is that they can be removed easily after *ex vivo* manufacturing using magnets similar to existing clinical protocols in T cell manufacturing. This biomaterial was synthesized with research-grade ingredients, with commercially available GMP-grade equivalent, and this 3D environment better maintained MSC stemness compared to 2D tissue culture plates. When coupled with wireless DMS by magnetic fields, we found that MSCs cultured in the magnetic hydrogel showed higher proliferation rate, enhanced production of growth factors, and controlled differentiation into osteogenic lineage (Scheme 1). We found that DMS enhanced matrix-integrin β1 interactions which induced MSCs spreading and formation of focal adhesion sites to activate focal adhesion kinase (FAK) and cytoskeleton contractility, and influenced cell activities via YAP nuclear localization and *FAK-ERK* pathway. Overall, this study demonstrates the potential of using biocompatible hydrogel technology to provide a 3D dynamic environment and enhance MSC functions including maintaining cell stemness, improving cell proliferation, directing cell differentiation, and growth factor secretions to overcome challenges associated with manufacturing MSCs in 3D biomaterials. We believe that this 'all-in-one' technology that integrates MSC culture to manufacturing and delivery/therapy offers a paradigm shift to existing standards in MSC therapy, especially for applications requiring few but high quality MSCs.

2. Materials and methods

2.1. Synthesis of gelatin methacryloyl (GelMA)

Gelatin methacryloyl (GelMA) was synthesized and modified according to previously reported method [38,39]. Briefly, gelatin from porcine skin was dissolved and stirred in phosphate buffer solution at 60 °C, and subsequently methacrylic anhydride (MA; 276685,

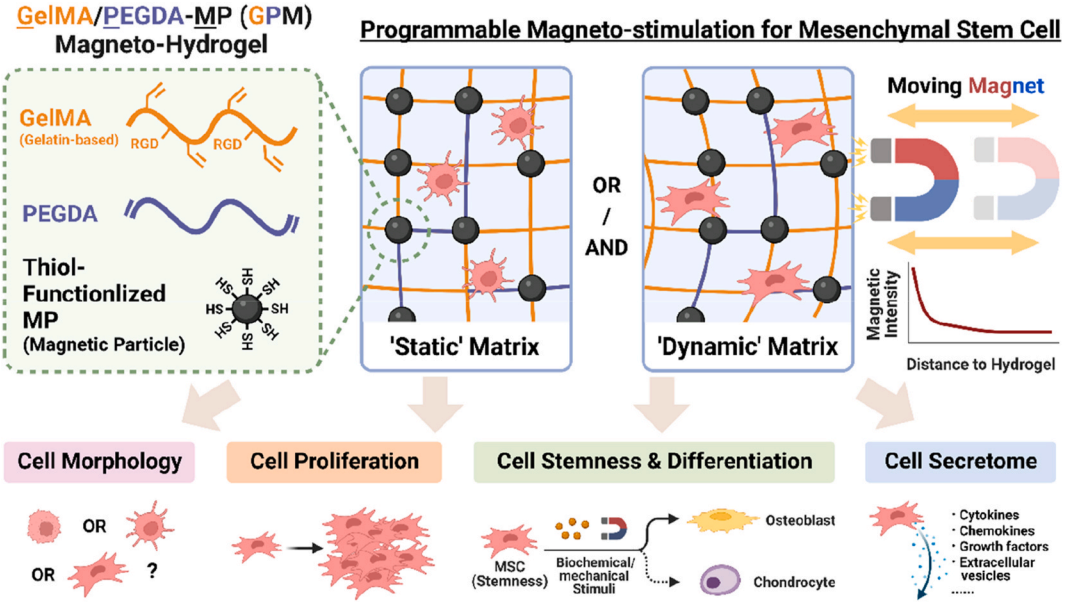

Scheme 1. Schematic illustration of GelMA/PEGDA-MP (GPM) magnetic hydrogel to provide dynamic mechanical stimulation (DMS) to influence mesenchymal stem cell (MSC) morphology, proliferation, stemness, differentiation, and secretome profile.

Sigma-Aldrich) was added dropwise and stirred for at 60 °C in dark. After a 4-h reaction, the mixture was centrifuged to remove surplus MA and the supernatant was added in dialysis tubing (10 K MWCO, 22 mm, Thermo Fisher) and placed in deionized water at 40 °C in an oven. Excess water was removed through lyophilization (Freeze Dryer, LyoLab 10S, Qingdao Antech Scientific CO., LTD) and final product was stored in −20 °C fridge.

2.2. Chemical characterization of polymers

Proton Nuclear Magnetic Resonance spectroscopy (^{1}H NMR; AVII400, Bruker) and Fourier Transform Infrared Ray spectroscopy (FTIR; VERTEX 70, Bruker) were conducted to validate the reactions between gelatin and MA, as well as the presence of functional groups in the end products. For ^{1}H NMR, it was recorded using 400 MHz Spectrometer at 25 °C in deuterium oxide (DLM-4-100, Cambridge Isotope Laboratories Inc.). Degree of substitution on GelMA (i.e., MA grafting rate) can be calculated through the signal ratios of proton on the unsaturated bonds by the equation [40,41]:

$$\%Degree\ of\ Substitution = \frac{\frac{\int Vinyl(b)}{2}}{\frac{\int Phenylalanine(a)}{5}} \times 100\% \quad (1)$$

where $\int Vinyl(b)$ is the integrated ratio of ^{1}H proton on grafted unsaturated bonds (peak b), and $\int Phenylalanine(a)$ is the integrated ratio of ^{1}H proton on phenylalanine group (peak a). The degree of substitution can also be represented by peak d which is related to the content of lysine methylene [42].

As the MA may react with the amino groups on gelatin backbone, which is a key motif for RGD sequence (i.e., tripeptide Arginine-Glycine-Aspartate), $\%NH_2$ was calculated with the equation below to select the best reaction ratio of GelMA macromolecules:

$$\%NH_2 = \frac{\frac{\int lysine\ (c)}{2}}{\frac{\int Phenylalanine(a)}{5}} \times 100\% \quad (2)$$

where $\int Lysine\ (c)$ is the integrated ratio of ^{1}H proton on unreacted lysine bonds (peak c).

2.3. Preparation of GPM hydrogel

GelMA and PEGDA solid samples were added into Dulbecco's Phosphate Buffered Saline (DPBS; D8537, Sigma-Aldrich), with desired final mass concentration. The solution was placed in 40 °C oven and stirred thoroughly to ensure that the macromolecules were completely dissolved. Subsequently, desired concentration of MPs and photo-initiator, Lithium phenyl-2,4,6-trimethylbenzoylphosphinate (LAP; VLLP0001, Cellink) were added into the solution and stirred homogenously. The precursor solution was immediately used for the subsequent steps which the solution and was exposed to ultraviolet (UV) lamp (EFL-LS-1601-405, EngineeringForLife) for 60 s. The UV lamp was set at wavelength of 405 nm and intensity of 25 mW/cm^2, which does not cause adverse effect to the cells. To avoid MP aggregation and sedimentation in the hydrogel network, in this work, particles were first treated by ultrasonic dispersion, and resuspended multiple time during mixing, followed by quick/efficient UV photo-crosslinking.

2.4. Characterization of GPM hydrogel

The hydrogel photo-gelation was measured with a rheometer (DHR-2, TA instrument). Accompanied by a 20-mm diameter parallel geometry (108940, TA instrument), the storage modulus (G′) and loss modulus (G″) of hydrogel samples before and after UV exposure were measured, as functions of test time. The mechanical features of hydrogel with different polymer or MP concentrations were measured with the rheometer, which the storage modulus (G') of hydrogel samples were measured with frequency sweep [43]. The elasticity of hydrogel was tested on compression testing machine (EZ-SX, SHIMADZU), by conducting 100 loading-unloading cycles (30s of 50% strain compression loading, 30s holding, 30s unloading to initial state, and 30s holding). The hydrogels were cut into cylindrical pieces (9.0 mm in diameter and 5.0 mm in height) and compressed by 15-mm diameter parallel geometry.

The structural features of hydrogel were analyzed by scanning electron microscope (SEM; JSM-6701F FEG, JEOL), and the morphology of MP was captured by transmission electron microscope (TEM; JEM-1400Flash, JEOL). The pore size of the dried hydrogel scaffolds and particle size were analyzed by ImageJ. The 3D distribution of loaded MPs (fluorescent-labelled) was characterized by confocal microscope (LSM710, Zeiss) and the data was analyzed by ImageJ and Imaris (version 9.7). Additionally, Zetasizer (ZEN360, MALVERN Instruments Limited) was used to test the hydrodynamic diameter of MPs. The magnetic features of the GPM hydrogels with various MP concentration were characterized by superconducting quantum interference device (SQUID) magnetometer (MPMS3, Quantum Design Inc.) with a maximum applied magnetic field of 20 kOe at room temperature.

For biomedical and clinical application, it is critical to study gel biostability and degradation profiles under physiological conditions [44]. The hydrogel constructs were immersed in DPBS solution (pH 7.4) in 24 well plate and placed in a shaking incubator (ZWY-100H, LABWIT) at 37 °C. After removing residual solution on the gel surface, the hydrogels were weighed at desired time points, and the swelling ratio of hydrogels (S) represented the condition of biostability was calculated by the following equation:

$$\%\ Swelling\ Ratio = \frac{S_t}{S_0} \times 100\% \quad (3)$$

where S_0 is the weight of the hydrogel on day 0, and S_t is the weight of the hydrogel after culturing for a desired period.

To determine the *in vitro* degradability, samples were freeze-dried and weighed at desired time points. The mass retention of hydrogels (W) representing the condition of degradation was calculated by the following equation:

$$\%\ Mass\ Retention = \frac{W_t}{W_0} \times 100\% \quad (4)$$

where W_0 is the weight of the initial lyophilized hydrogel, and W_t is the weight of the lyophilized hydrogel after culturing for a desired period.

2.5. Cell culture

After cell isolation and purification, rat MSCs were expanded in fresh MEM-α medium supplemented with 10% fresh Fetal Bovine Serum (FBS) and 1% Penicillin-Streptomycin (P/S; Antibiotic-Antimycotic), at 37 °C and 5% CO_2 cell incubator. Subculture was performed at 70–80% confluency. Cells at passage 3 to 5 were used for all further experiments. All reagents were obtained from Gibco.

2.6. Cell proliferation

Proliferation of encapsulated MSCs was measured by DNA quantification assay using Quant-iT™ PicoGreen™ dsDNA Assay Kits (P11496, Thermo Fisher) [45]. Briefly, the hydrogels were treated by Cell Collect G kit (LR0200000010, Cellink) which contained collagenase to degrade hydrogel constructs. The cells were then lysed by RIPA lysis buffer (ab156034, Abcam). The Pico-green working solution and diluted DNA sample solution were mixed followed by 5-min incubation. The fluorescent intensity of each specimen was measured using multimode microplate reader (SPARK, TECAN) at 480 nm excitation and 520 nm

emission.

2.7. Biocompatibility and cytotoxicity of GPM hydrogel

The 3D distribution of encapsulated cells (DAPI-labelled) and loaded MPs (fluorescent-labelled) were characterized by confocal microscope (LSM710, Zeiss) and the data was analyzed by ImageJ and Imaris (version 9.7). To confirm the biocompatibility of hydrogel and influence from external magnetic field, Cell Counting Kit 8 (CCK8; ab228554, abcam) were used to test cell metabolism. Cells were cultured in hydrogel with different conditions including pure GelMA/PEGDA hydrogel (without MP), GPM hydrogel, and GelMA/PEGDA hydrogel (without MP) with magnet, and the CCK8-treated medium was measured on day 0, 1, 4, 7, and 14 by spectrophotometer (Multiskan Go Type 1510, Thermo Fisher) at 460 nm. To understand whether MPs removal after *ex vivo* manufacturing has negative effects on cells, MSCs were collected from GelMA/PEGDA (pure hydrogel without MPs) and GPM hydrogel (with MPs), respectively. MPs were removed by external block magnet, and cell metabolism was measured by CCK8. In addition, to assess the cytotoxicity of the GPM hydrogel, the samples were assayed with LIVE/DEAD™ Cell Imaging Kit (R37601, Thermo Fisher) at desired time points (Day 0, 1, 4, 7, and 14) and imaged by confocal microscope (FV3000, Olympus).

2.8. Alkaline phosphatase (ALP) activity

ALP activity is a marker of early-stage osteogenic differentiation [46]. ALP assay kit (MK301, TaKaRa) was used to analyze the osteogenic differentiation of MSC in the magneto-dynamic hydrogel. Briefly, the hydrogels were degraded to isolate the differentiated cells. The cells were then lysed by extraction solution and then incubated with *p*-nitro-phenyl phosphate (pNPP) in ALP buffer under 37 °C for 60 min. Following that, 0.5 M NaOH solution was added to stop the reaction and the absorbance was taken at 405 nm. Amount of ALP was extrapolated from standard curve of bone-specific ALP samples and normalized to DNA content in the samples.

2.9. Sulphated glycosaminoglycan (sGAG) assay

Sulphated glycosaminoglycan (sGAG) secretion is an important event during MSC chondrogenic differentiation. In this work, sGAG assay kit (B1000, Blyscan™) was used to analyze the chondrogenic differentiation of MSC in the magneto-dynamic hydrogel. Briefly, the hydrogels were degraded and then cell/hydrogel suspension solution was collected. Blyscan dye reagent was then added, which a sGAG-dye complex would form and precipitate out from the soluble unbound dye. After removing the supernatant, dissociation reagent was then added to release the bound dye into solution and finally measured the absorbance on 656 nm. The standard curve was made by glycosaminoglycan standard reagent and normalized to DNA content in the samples.

2.10. In vitro angiogenesis assays

Primary vein endothelial cells (VECs) were cultured in endothelial cell media kit (C22111, PromoCell) and cells from passages 3 to 5 were used for the *in vitro* VEC assays. Each conditioned medium was collected from MSC-laden hydrogel and mixed with growth factor-free VEC culture medium and used for *in vitro* VEC assay. Based on previous study, VECs were unable to grow in pure conditioned medium and a minimal amount (70%) of VEC culture medium was needed to keep cell viable [47]. Commercial growth factor-supplemented cell culture medium was served as the positive control in the experiment. To study the *in vitro* VEC proliferation for 1 and 4 days, collected conditioned medium mixtures were used to supplement the culture medium, and normalized to DNA content in the samples.

The effect of dynamic cultured MSC conditioned medium on chemotactic migration of VECs was determined by u-Slide Chemotaxis (#80306, ibidi), based on the manufacturer's protocol. Briefly, cell suspension was added into each chip center chamber. After 6 h, seeded cells were attached at the chip chamber surface, growth factor-free culture medium was then introduced in the lower chamber, while the upper chamber was infused with each collected conditioned medium mixture. Following that, the migratory behaviors of VECs were monitored by microsystem (DMIL LED Fluo, Leica) for time-lapse imaging. For each group, the migratory route was tracked by FastTrack AI Image Analysis (ibidi) and the values were obtained by manual tracking using the ImageJ Manual Tracking Plugin. In addition, we also used 'wound migration' model to verify the chemotaxis driven by MSC conditioned medium, which was conducted on culture-insert 2 well in u-Dish (#81176, ibidi), based on the manufacturer's protocol. Briefly, VECs were seeded in each insert well and cultured until the area was mostly occupied. Following that, the two culture-insert wells were removed and rinsed, the cell-uncovered gap between the inserts mimicked the endothelial wound site. Then, the cells were cultured with MSC conditioned medium and were imaged with by microsystem (DMIL LED Fluo, Leica) at 2, 5, 10, and 24-h post-treatment, and wound closure rates were calculated by ImageJ.

The effect of the various conditioned medium on angiogenesis of endothelial cells was evaluated by a fibrin gel bead sprouting assay, performed with modifications [48]. Briefly, Cytodex 3 microcarrier beads (c3275, Sigma-Aldrich) were coated with VECs in endothelial cell growth medium (EGM-2 BulletKit Medium, CC-3162, Lonza). The cell-bead suspension was agitated and allowed to adhere overnight. Coated beads were subsequently suspended in fibrinogen solution at a concentration of 500 beads/ml. After generating a clot, solidified gels were then topped up with desired conditioned or control medium. Subsequently, the cells were incubated overnight at 37 °C, 5% CO_2 and observed for sprout formation after 6 h using a phase contrast microscope (CKX53, Olympus).

In vitro VEC tubular network formation assay was performed using the μ-Slide Angiogenesis (#81506, ibidi), based on the manufacturer's protocol. Briefly, each well was first coated with Matrigel (#356231, BioLab) and seeded with cells, supplied with pre-determined medium. Samples were then incubated for the formation of capillary-like tube and subsequently imaged using the confocal microscope (FV3000, Olympus) under brightfield and fluorescent laser (VECs were labelled by blue DAPI and green phalloidin (A12379, Thermo Fisher)). Brightfield images were analyzed with the FastTrack AI Image Analysis (ibidi). The number of loops and branches as well as total tube length were computed to quantify the extent of tube formation.

2.11. Transfection of integrin β1 siRNA

To verify the role of integrin β1 in MSC activities and features, commercial integrin β1 siRNAs were designed and obtained from GenePharma Inc. Lipofectamine 2000 Transfection Reagent (Lipo2000; 11668019, Thermo Fisher) was used as cargo carrier for gene transfection to knockdown integrin β1. After diluted in OPTI-MEM (31985070, Thermo Fisher), MSCs were transfected in the complex using a siRNA (μg) to Lipo2000 (μl) ratio of 1:2 for 12 h. After desired post-culture and stimulation, the efficacy of transfection and knockdown was monitored by fluorescent microscopy with the help of fluorescent siRNA control and Western blot analysis.

2.12. Statistical analysis

All experimental data were reported as the mean ± standard deviation. Statistical analysis for experimental data involved in this paper was conducted by using T-test or one-way ANOVA and followed by pairwise comparison with Tukey's multiple comparisons test using SPSS statistical software (Version 26). The sample-to-sample correlation was analyzed by Pearson correlation coefficient which conducted by

OriginPro. Single asterisk (*) indicates $p < 0.05$, double asterisks (**) indicates $p < 0.01$, triple asterisks (***) indicates $p < 0.001$, quadruple asterisks (****) indicates $p < 0.0001$, and n.s. indicates not significant.

3. Results

3.1. Design and characterization of GPM hydrogel

To provide a biocompatible environment, gelatin, a major constituent of the naturally occurring ECM, was used as the main component of the hydrogel. Methacrylic anhydride (MA) were reacted with lysine and hydroxylysine groups (primarily to amino group) on the gelatin, and the grafted vinyl groups were crosslinked to form hydrophilic GelMA hydrogel networks [38,39]. Successful modification was supported by characteristic peaks via ^{1}H-NMR (Fig. S1). Importantly, RGD peptide sequence (i.e., tripeptide Arginine-Glycine-Aspartate) on the gelatin provided a site for cell-ECM adhesion [49,50], and it was critical to preserve adequate RGD motifs on GelMA while having high degree of substitution (%DS) of grafted unsaturated bonds. After balancing the % DS and RGD motif amount, GelMA 1:0.125 (g/ml) was selected as the optimal condition (Fig. S2). In addition, considering the need to maintain biostability of the artificial matrix, poly (ethylene glycol) diacrylate (PEGDA), a non-biodegradable but biocompatible macromolecule was included in the hydrogel network [51]. The double bond (C=C) on PEGDA made it easy to integrate with GelMA components under photo-crosslinking, and compared to pure GelMA hydrogel, GelMA/-PEGDA mixtures had more stable profile with longer degradation period and lower swelling ratio (Fig. S3).

To enable DMS by external magnet, thiol-functionalized magnetic particle (MP; maghemite core coated with sulfhydryl) were incorporated into the hydrogel network. Upon UV irradiation, the GPM hydrogel liquid precursor solution became an injectable hydrogel (Fig. 1a and S4), and its storage moduli or stiffness could be controlled by changing polymer concentration (Fig. 1b). Instead of physical blending MPs into the hydrogel which might lead to leakage and cell cytotoxicity, MPs were grafted onto GelMA and PEGDA backbone by thiol-ene click reaction as supported by the carbon-sulfur chemical bond (Fig. S5) [52–54], to minimize MPs leakage from hydrogel construct (Fig. 1c and S6). As shown in Fig. 1d, relatively large-sized MPs with average diameter of ~4.1 μm were used here to enhance sensitivity to magnetic

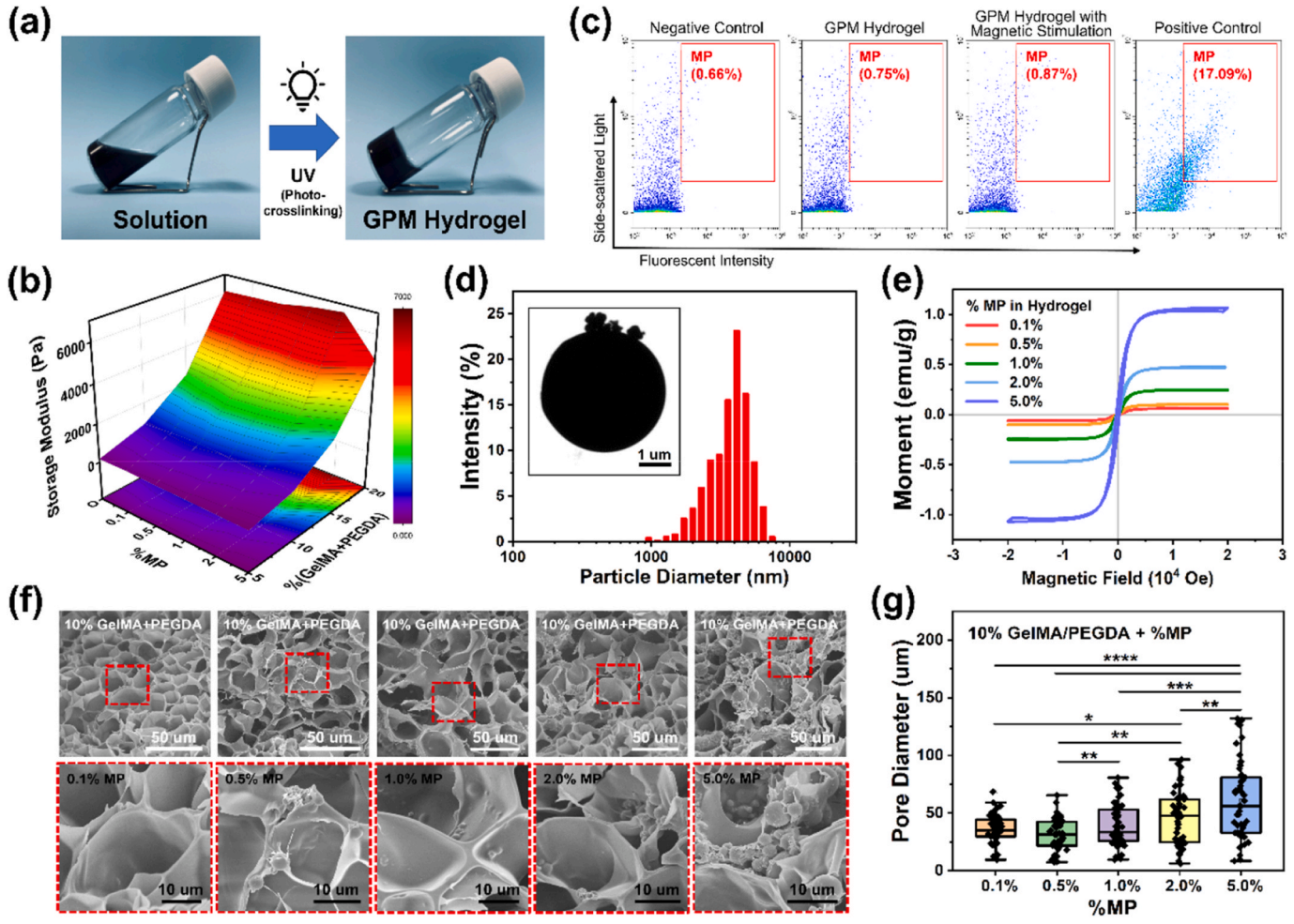

Fig. 1. Characterization of GelMA/PEGDA-MP (GPM) hydrogel. **(a)** Photographs of GPM liquid precursor becoming hydrogel after UV-mediated photo-crosslinking. **(b)** Storage modulus of GPM hydrogel with different polymer and MP concentrations. **(c)** Flow cytometric analysis showing negligible leakage of magnetic particles (MPs) from the hydrogel with/without mechanical stimulation. **(d)** Dynamic Light Scattering (DLS) revealed size of magnetic particle (MP) to be ~4.1 μm. Inserted image: Transmission Electron Microscopy (TEM) image of MP with a spherical morphology. **(e)** M − H curves of GPM hydrogels with different MP concentrations via superconducting quantum interference device (SQUID) analysis, showing that GPM hydrogels were magneto-responsive. **(f)** Scanning Electron Microscopy (SEM) images of porous network in GPM hydrogel with varying MP concentrations. As the MP amount increased, the hydrogel network was gradually perturbed with decreased network crosslinking rate and enhanced pore sizes. **(g)** Average pore diameter of GPM hydrogel network with different MP concentrations. All box plots indicate median (middle line), 25th, 75th percentile (box) and the lowest (respectively highest) data point (whiskers). Statistical significance is indicated as *$p < 0.05$, **$p < 0.01$, ***$p < 0.001$, and ****$p < 0.0001$.

fields and minimize nanomaterial-associated cytotoxicity due to unintended endocytosis *in vivo* [55,56]. The magneto-responsiveness and superparamagnetic property of GPM hydrogel were also supported by superconducting quantum interference device (SQUID) analysis (Fig. 1e). Using MPs is also advantageous as they can be removed easily after *ex vivo* manufacturing using magnets and have minimal effects on cell metabolism and behaviors (Fig. S7), similar to existing clinical protocols for using and removing MPs in T cell manufacturing.

Based on the SEM images (Fig. 1f and S8), GPM hydrogels had uniform MP distribution with an interconnected porous network to provide ample space for nutrient diffusion, cell growth, and migration. The porosity and network density were closely related to the concentration

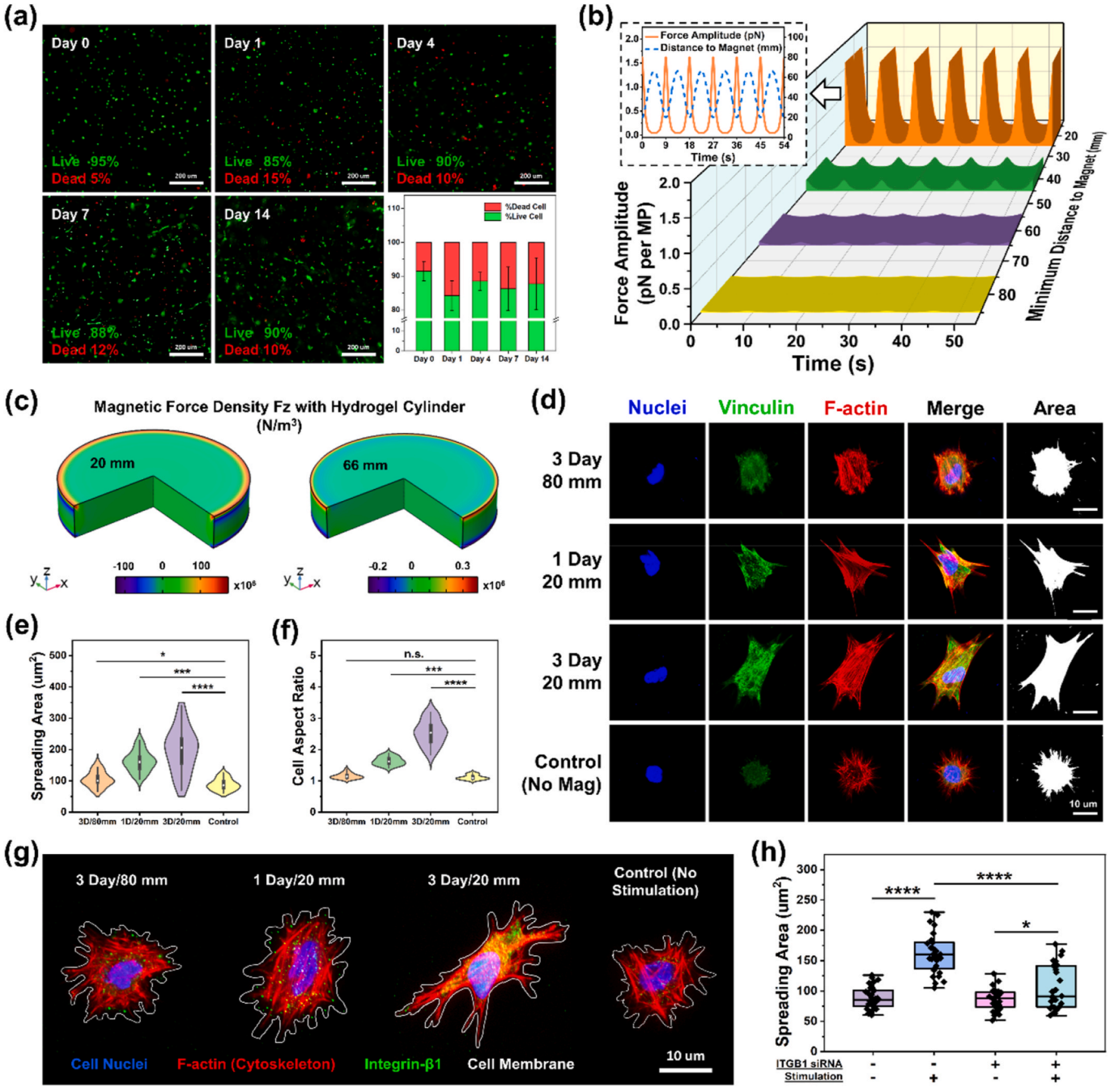

Fig. 2. Cell growth and morphology of bone marrow-derived mesenchymal stem cells (MSCs) in GPM hydrogel. (**a**) Live-dead staining of MSCs encapsulated in hydrogel from 0 to 14 days, indicating high biocompatibility of GPM hydrogel. (**b**) Profile of magnetic force applied to GPM hydrogel from the dynamic magnetic device with the magnet movement ranging from 20 to 66 mm. (**c**) Multiphysics modelling of DMS-induced force distribution within cylinder hydrogel (magnet-hydrogel distance are 20 and 66 mm), suggesting that the force is uniform within hydrogel construct. (**d**) Fluorescent images of MSC morphology and cytoskeletons under different culture conditions, showing that dynamic mechanical stimulation (DMS) promoted MSC spreading. Violin plot of MSC (**e**) spreading area and (**f**) cell aspect ratio under DMS. Internal box plots show medians with interquartile range and whiskers. (**g**) Fluorescent images of MSC cytoskeleton and integrin protein level showing that DMS promoted higher surface expressions of integrin-β1 linked to MSC spreading. (**h**) Box and whisker plots of MSC spreading area upon siRNA inhibition indicating that integrin β1 plays a key role in cell spreading in DMS. All box plots indicate median (middle line), 25th, 75th percentile (box) and the lowest (respectively highest) data point (whiskers). Error bars represent standard deviations based on four biological replicates, in which at least 10 MSC single cells were analyzed for each replicate. Statistical significance is indicated as *p < 0.05, **p < 0.01, ***p < 0.001, ****p < 0.0001, and n.s. is not significant.

of polymer and MP [57]. In high %MP hydrogel, some MP aggregations were observed in the hydrogel scaffold due to inevitable MP-MP magneto-attraction, but only slight aggregation was observed in low %MP groups (i.e., 0.1%, 0.5%, 1.0%). Also, we found that a trace amount of thiol-functionalized MPs could serve as additional cross-linkers to heighten polymer network stability [58], but when more MPs reacted with the polymer unsaturated groups, intermolecular interactions and crosslinking were disrupted resulting in a sharp increase of pore size (Fig. 1g). When MPs were in excess, the microscopic structure of the hydrogel network became disorganized, therefore influencing the overall mechanical properties of the hydrogel (Fig. 1b). Thus, 1% MP and 10% polymer (GelMA/PEGDA) were used for future works due to optimal biophysical and biochemical features including mechanical stability, reduced degradation rate, minimal particle leakage and optimal pore size for cell growth and spreading. Importantly, all ingredients used for this GPM hydrogel are low-cost, biocompatible, and with commercially available GMP-grade equivalent, which makes it possible for future clinical-grade cell manufacturing.

3.2. Healthy growth of MSC in 3D scaffold with dynamic mechanical stimulation

Isolated primary rat bone marrow-derived MSCs had stable stemness (Fig. S9) and multi-lineage differentiation potential (Fig. S10). To understand how 3D environment and dynamic activation influence cell growth and biofunctions, we seed MSCs in our GPM hydrogel, and as shown in Fig. S11, MSCs and MPs were distributed randomly in the hydrogel to generate uniform magneto-induced DMS to cells. Fluorescent images revealed that cells adhered to the hydrogel network and MPs were not internalized despite being in proximity to MSCs [59–61]. When compared to MP-free hydrogel (i.e., GelMA/PEGDA hydrogel), the addition of trace amounts of MPs in GPM hydrogel had no obvious effect on cell survival and metabolism (Fig. S12). Live-dead staining also revealed exceptional biocompatibility (Fig. 2a). In addition, importantly, magnetic DMS had no noticeable negative effect on cell growth (Fig. S12).

To provide DMS, a cyclically rotating permanent magnet with a low frequency of 0.10 Hz was applied to the MSCs for 4 × 30 min interval. As the strength of magnetic field is inversely proportional to the distance between the magnet and cells, when the magnet block moved close to the hydrogel construct, MPs covalently bonded to the hydrogel scaffold were magneto-attracted, resulting in the contraction and compression of hydrogel network; when the magnet rotated away, MPs were released from the magneto-attraction and the hydrogel network restored to its original shape due to the viscoelastic feature of GPM hydrogel (Fig. S13).

This dynamic magneto-attraction/releasing on GPM hydrogel induced a dynamic environment with cyclic mechanical stimulation to encapsulated MSCs, and the force amplitude could be easily tuned by adjusting the distance between hydrogel and magnet block (Fig. 2b). Based on multiphysics modelling, under DMS (hydrogel-magnet distance from 20 to 66 mm), we found the hydrogel construct had uniform spatial distributions of the magnetic force density along the axial direction (Fig. 2c and S14), which is critical for cell manufacturing. Note that 20 mm and 60 mm refer to the closest distance between the top of the magnet and bottom of the magnet to the hydrogel, respectively. We decided to build a multiphysics model with the closest distance as the magnetic field strength decay is most significant (Fig. S34). The modeling revealed non-uniform stress around the lateral surface of hydrogel caused by hydrogel lateral deformation and resistance force from mold wall (Fig. S15). As this area is negligible, >99% of cells (based on volume ratio calculation) is not expected to be affected by non-uniform stress (Fig. 2c and S14).

3.3. Dynamic mechanical stimulation promotes MSC spreading via ECM-integrin β1 interaction

To determine the effects of DMS on MSC growth and biofunctions, cells were cultured in GPM hydrogel with DMS, and the amplitude of the mechanical stimulation was adjusted by stimulation length (day) and force amplitude (distance between hydrogel and magnet). The cellular cytoskeletal organization and expression were visualized after four different mechanical stimulation regimens (Fig. 2d). MSCs under stronger DMS were elongated and polygonal, with ~2.2-fold increase in cell area and larger cell shape factors (i.e., larger cell aspect ratio and smaller circularity) than MSCs under static cultivation which were smaller and spherical (Fig. 2e,f and S16) likely attributing to focal adhesion maturation and cytoskeleton assembly as demonstrated in previous works [62–65]. As shown in Fig. 2d and S16, stronger DMS resulted in more pronounced actin stress fibers (i.e., F-actin) and punctuated vinculin accumulation (a key component of focal adhesion site) in MSCs. The enhanced expression of vinculin likely connected the F-actin bundle to focal adhesion site, leading to stronger cell adhesion and ultimately influenced cell morphology [64,66].

We hypothesize that MSCs which adhered onto RGD ligands on the hydrogel network transduced the external mechano-signals to regulate cell behaviors in the presence of DMS [65,67]. To verify our idea, we fluorescently stain integrin receptors, which are the well-studied cell surface transductors. In this work, among them, we primarily focus on integrin β1, as it is the most prominent integrin receptor (half of integrin heterodimers are made up by integrin β1 [68]) and it has a critical role in cell attachment to the ECM [69,70]. As shown in Fig. 2g and S17, more punctuated integrin β1 stained on the membrane of MSCs which experienced stronger DMS, demonstrating promoted ECM-integrin interaction. This is further supported by partial integrin β1 knockdown using siRNA transfection which showed that when the expression level of integrin β1 was reduced, DMS had less effect on MSC morphology and focal adhesion formation (Fig. 2h and S18). There are recent studies using large gradient high magnetic field to affect cell morphology. However, as the magneto-stimulation pulse and length used in our work was relatively lower and shorter [71–73], MSCs had no obvious spreading and increased focal adhesion formation under the influence of pure magnetic field (Fig. S19), confirming that magneto-induced DMS is the primary reason for our observation.

3.4. Activated integrin-related pathway under dynamic mechanical stimulation

In addition to controlling cell morphology, integrin is a critical regulator of MSC biofunctions. To identify the relevant mechanisms, we profiled mRNA expressions (Fig. 3) and gene-gene correlations (Fig. S20) using MSCs from four rat donors under different dynamic/static cultures. Stronger DMS induced higher expressions of *ITGB1* which could be attributed to stronger RGD-integrin interaction, resulting in the formation and maturation of focal adhesion site, with increased FAK phosphorylation (i.e., *PTK2*) and *SRC* expressions which are both implicated in integrin signaling. In addition to *ITGB1*, other integrin receptors such as *ITGA1*, *ITGA2*, and *ITGA5*, also showed upregulated gene expression under strong DMS, demonstrating their potential participation in mechano-transduction.

Stronger DMS also led to higher expression level of *MKI67*, a marker of cell proliferation and growth, that is associated with enhanced *YAP1* expression due to downregulation of Hippo pathway. Additionally, stronger DMS enhanced *MAPK* which is part of the *FAK-ERK* pathway to improve MSC paracrine activities such as improved VEGF expression [74]. This is aligned with our findings that *ERK* activation also promoted an increase in expression levels of osteogenic markers (e.g., *BGLAP*, *SP7*) when MSCs are cultured in osteogenic medium [75] and decrease in expression levels of chondrogenic genes (e.g., *ACAN*, *COL2A1*) in chondrogenic medium.

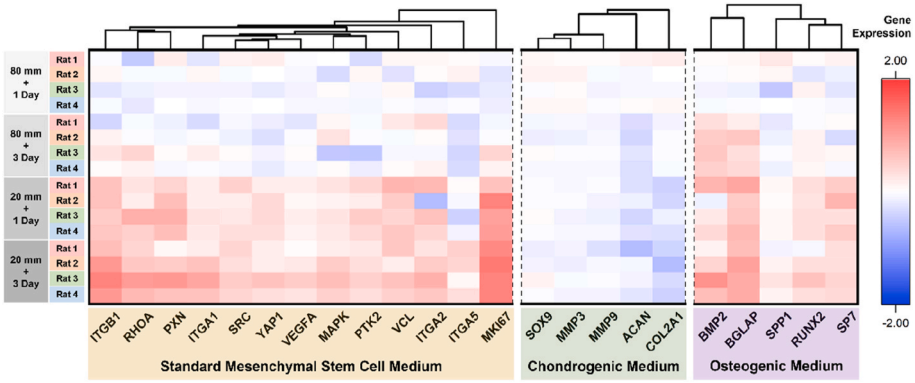

Fig. 3. The gene expression of potential activated integrin-related pathways under dynamic mechanical stimulation (DMS). Heatmap showing changed gene expression profile of bone marrow-derived mesenchymal stem cells (MSCs) in different DMSs. The dynamic force is conducive to MSC spreading, proliferation, and secretion in the standard medium. DMS has a positive effect on cell osteogenesis while it impeded cell chondrogenesis. Each row represents the gene expression profile for MSCs from rat donors in different conditions, and each column represents a gene. Hierarchical clustering dendrogram showing Pearson correlation between different genes.

Collectively, gene expression analyses support that DMS influenced MSC behaviors via RGD-integrin interaction, and stronger DMS intensity promoted higher expression of genes to induce MSC cell spreading, proliferation, paracrine activities, and directing MSC differentiation into specific osteogenic lineages.

3.5. 3D dynamic matrix optimizes MSC quantity and quality

Clinical protocols usually require *in vitro* MSC expansion to get sufficient cell numbers, especially for autologous therapy which uses patient's own cells. We found that DMS shows promise to promote MSC proliferation as stronger DMS (i.e., stronger magnetic intensity and longer stimulation duration) in GPM hydrogel promoted cell growth (Fig. 4a and b). To evaluate the DMS intensity, we set a coefficient parameter, Magneto-stimulation index, which is calculated by multiplying 'magnetic force amplitude' with 'stimulation duration'. This result is in good agreement with higher *MKI67* expression (Fig. 3) and YAP activation with reduced levels of its phosphorylated state under DMS (Fig. 4c) and had higher nuclear localization rate (Fig. 4d). The key contribution of integrin β1 on mechanotransduction was supported by its partial knockdown, with lower increase of *YAP1* and *MKI67* genes (Fig. S21).

Besides cell quantity, another key consideration for manufacturing is to generate high quality MSCs with stable self-renewal and differentiation potential. Conventional methods using 2D tissue culture plates can achieve high cell expansion rate, but these platforms reduce stem cell potency [10]. One potential reason is that MSCs spread excessively on the 2D culture plate. On culture plates, some MSCs transit from small, spindle-like phenotypes to big, flat-like ones (Fig. S22), and these cells lose stemness features during passaging (Fig. S23) [76]. 3D hydrogel culture that better mimic *in vivo* microenvironment can overcome this problem. As shown in Fig. 4e and S24a, 3D cultured MSCs had ~1.5-fold higher expression of cell surface stemness marker (CD90) than those cultured on 2D plate, albeit, with slightly low proliferation rate (Fig. 4f). DMS could enhance MSC proliferation but this could also reduce MSC stemness as shown by decreased CD90 expression (Fig. 4e and S24b), increased nuclei size (Fig. S25) [77] and reduced *SOX2* and *OCT4* gene expressions (Fig. S26) which are essential transcription factors for stem cell pluripotency and self-renewal [78].

We argue that it is significant to find a 'balance' and optimize cell quantity and quality during MSC manufacturing as existing platforms have their respective pros and cons. Here, based on our data, we set a coefficient parameter that is calculated by multiplying 'proliferation rate' with 'stemness marker intensity' to evaluate the effects of DMS on MSCs (i.e., PROLIFERATION * STEMNESS) [30]. Interestingly, we found that 3D hydrogel culture with a gentle mechanical stimulation (3Day/40 mm) exhibited an better effect than pure 2D or 3D culture (Fig. 4g). In other words, DMS can be optimized to improve MSC expansion with negligible reduction in stemness, suggesting a promising approach to optimize current MSC manufacturing protocols using DMS with 3D hydrogel.

3.6. Dynamic mechanical stimulation directs MSC differentiation

Harnessing the ability of MSCs to differentiate into bone-forming osteoblasts and cartilage-forming chondrocytes, this cell type has been widely used for bone and cartilage repair [7,79]. Inspired by the pivotal roles of mechanical stimuli for bone regeneration *in vivo*, herein, we explored how DMS can affect and direct MSC differentiation in our 3D scaffold. We found that the dynamic forces promoted MSC osteogenesis, and higher force amplitude and duration generated MSC population with preference for the osteogenic lineage (Fig. 5a and b). The activation of *FAK-ERK* mechano-transduction signalling was a key pathway to facilitate osteogenesis, with increased expression of osteogenic marker, RUNX2 and osteocalcin (OCN) (Fig. 5c and S27). Integrin β1, in this process, plays a key role in transducing the mechanical signals from external matrix, which was supported by partial knockdown and FAK inhibition (Fig. 5c and S28). Interestingly, we observed that DMS could promote MSC differentiation into tendon cells (Fig. S29). This could be attributed to similar features shared with osteogenesis including (i.e., mechanical loading environment [80]), ECM molecular deposition (e.g., collagen type I), and mechanotransduction (e.g., integrin-related pathway [81]). On the contrary, as shown in Fig. 5d–f, DMS was unconducive for MSC chondrogenesis as demonstrated by lower expressions of sulphated glycosaminoglycan (sGAG), aggrecan (ACAN) and collagen type II (Col II) under stronger DMS. These results recommend using a dynamic/static environment for bone/cartilage regeneration in manufacturing and clinics. In addition, morphology and spreading area have critical impacts on MSC differentiation behaviors. Recent studies have found that MSC with an elongated, spreading morphology have a higher degree of osteogenesis, while small, spherical one tends to chondrogenic differentiation [65,76,82–84], aligned with the previous findings driven by cytoskeletal changes [82,85].

Our finding indicates the possibility of directing MSC differentiation lineage using DMS. This is of great potential in multi-layer bone defect repair where there are two tight layers containing different cell types, for example, osteochondral interface at the knee joint (Fig. 5g) [26,86,87]. Thus, we developed a bilayer hydrogel scaffold with a MP-contained bottom layer (GPM hydrogel) which external magneto-mechanical force may drive MSCs towards osteogenesis (i.e., bone region), and a MP-free top layer (GelMA/PEGDA hydrogel) intended for chondrogenic differentiation (i.e., cartilage region) (Fig. 5h). Taking advantages of wireless manipulation of our system, although two MSC-contained layers are tightly bonded, MP-free layer remained under static environment. After 3-day exposure to the magnetic field, we found that DMS induced MSCs in 'bone region' to exhibit greater spreading and produce more collagen type I (Col I), while MSCs in 'cartilage region' displayed spherical morphology and higher

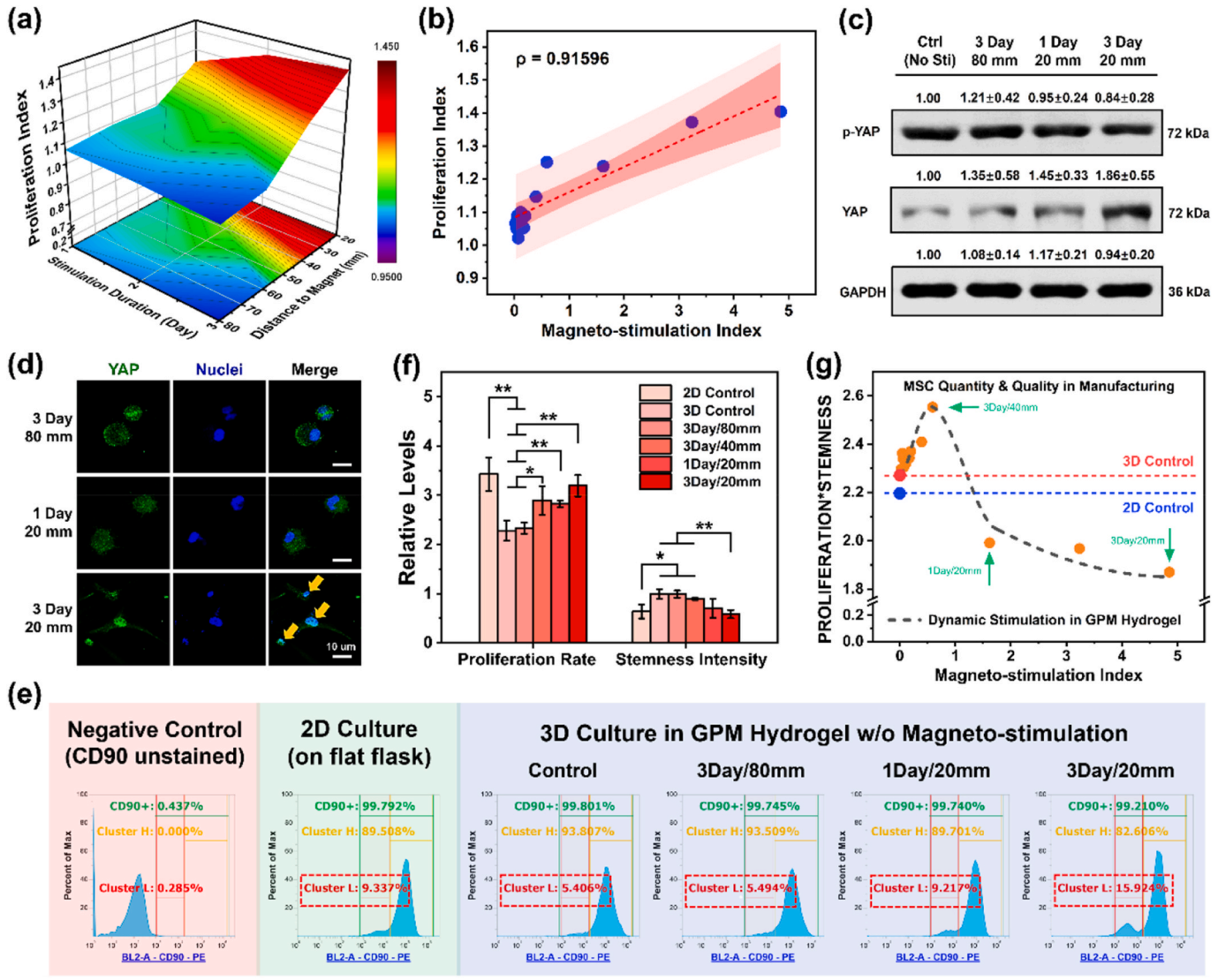

Fig. 4. Cell proliferation of bone marrow-derived mesenchymal stem cells (MSCs) in GPM hydrogel. (**a**) Parametric analysis of MSCs proliferation condition found that stronger and longer dynamic mechanical stimulation (DMS) better promoted MSC proliferation. (**b**) Strong positive correlation between cell proliferation and DMS (ρ, Pearson correlation coefficient). Magneto-stimulation index is obtained by multiplying 'magnetic force amplitude' with 'stimulation duration' which shows the DMS strength. (**c**) Western blot analysis that dynamic environment promotes MSC proliferation via YAP pathway that downregulates LATS-driven YAP phosphorylation and facilitates YAP nuclear localization rate. (**d**) Fluorescent images of YAP nuclear localization under different DMS conditions. (**e**) Flow cytometry of CD90 expression on MSC surface under different culture conditions. Data show that static and 3D environment better maintained MSC stemness. The red dashed outlines represent cell cluster with relatively lower CD90 expression, and this cell subpopulation was highest in 2D culture and 3D culture under strong DMS. (**f**) Bar graph showing that strong DMS (3Day/20 mm) improved cell proliferation while compromising MSC stemness, similar to 2D culture. (**g**) Graph of MSC manufacturing under different DMS conditions suggesting that 3D culture with gentle dynamic stimulation (low magneto-stimulation index) could produce MSCs with a better balance between cell quantity and quality (i.e., PROLIFERATION*STEMNESS). Statistical significance is indicated as *p < 0.05, **p < 0.01, ***p < 0.001, ****p < 0.0001, and n.s. is not significant.

expression of collagen type II (Col II) representing the differentiation preference towards chondrocyte (Fig. 5i and j). This differential preference to different lineages was not observed in the bilayer construct without magnetic stimulation (Fig. 5k), highlighting the promise of our strategy for engineering osteochondral tissue for direct use in therapy after manufacturing.

3.7. Dynamic mechanical stimulation enhances cell secretome for angiogenesis

Activation of mechanotransduction pathways have been shown to induce changes in MSC secretome such as improved production of pro-angiogenesis growth factors [74,88], including mechanical stimulation of MSCs to treat vascularization deficiency [47,89]. As shown in Fig. 6a and b, with GPM hydrogel, we found that DMS improved VEGF production and the amount was strongly correlated to the mechanical dose. This is associated with the activation of *FAK-ERK* mechanotransduction pathway where stimulated FAK increased ERK phosphorylation and downstream paracrine signalling (Fig. 6c). When MEK inhibitor was used to block the phosphorylation of ERK, no significant increase of VEGF was observed, demonstrating the key contribution of *FAK-ERK* pathway. DMS also increased the amount of bFGF, another potent inducer of angiogenesis and cell migration, in MSC secretome (Fig. S30). To further study the angiogenic effect of MSC secretome, we collected MSC conditioned medium under different stimulations and cultured it with vein endothelial cells (VECs). Conditioned medium with stronger DMS (i.e., 3Day/20 mm) induced higher VEC proliferation rate (Fig. S31) and better angiogenic sprouting and vascularization network

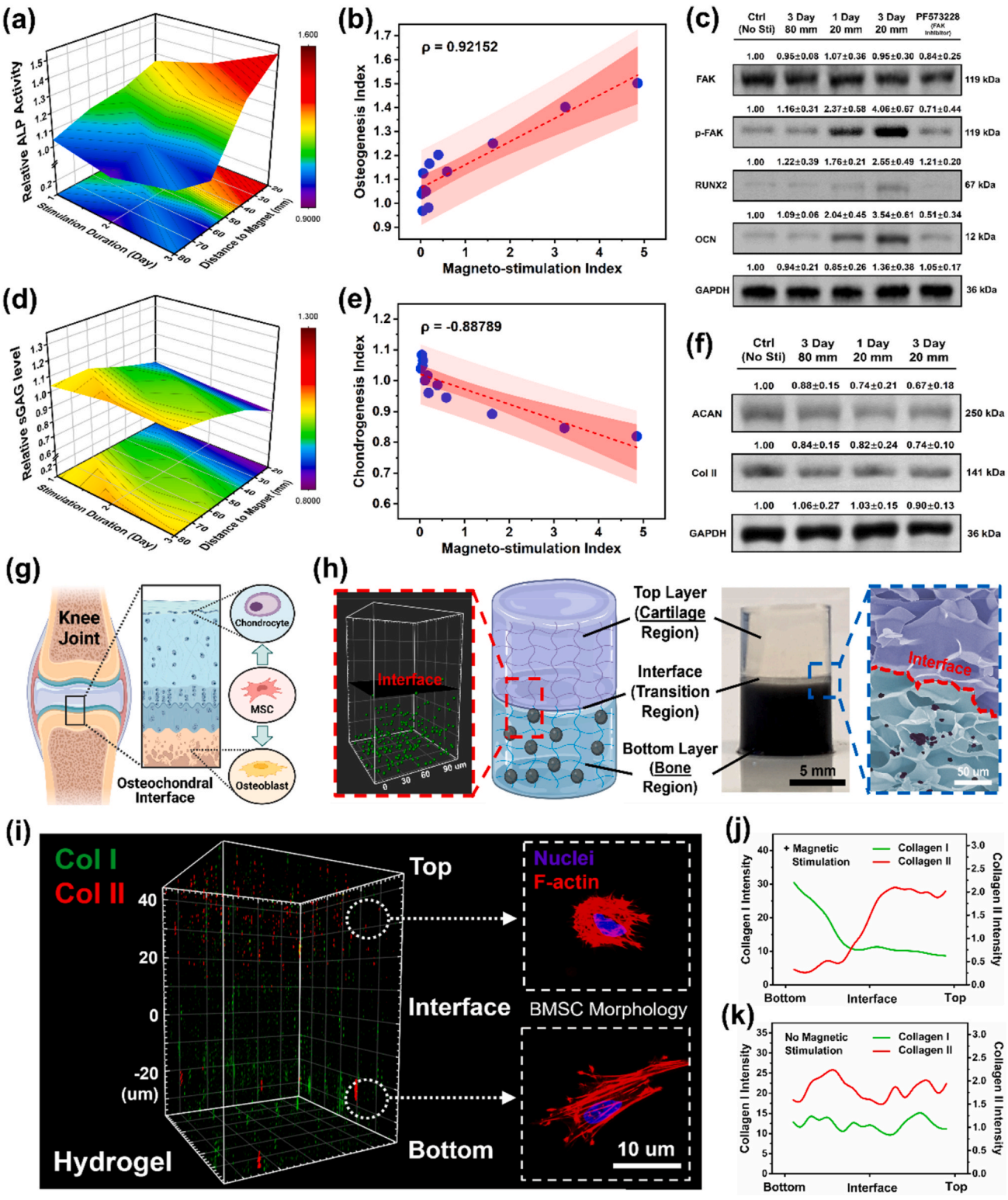

Fig. 5. Osteogenic and chondrogenic differentiation of bone marrow-derived mesenchymal stem cells (MSCs) in GPM hydrogel. (**a**) Parametric analysis of MSC osteogenic differentiation indicating that stronger and longer dynamic mechanical stimulation (DMS) favored osteogenesis. (**b**) Strong positive correlation between osteogenesis and external stimulation (ρ, Pearson correlation coefficient). (**c**) Western blot analysis showing that DMS promoted MSC osteogenesis via FAK pathway. (**d**) Parametric analysis of MSC chondrogenic differentiation indicating that stronger and longer DMS disfavored chondrogenesis. (**e**) Strong negative correlation between chondrogenesis and external stimulation (ρ, Pearson correlation coefficient). (**f**) Western blot analysis showing reduced chondrogenic marker proteins under dynamic conditions. (**g**) Schematic illustration of osteochondral interface on the knee joint. (**h**) Photos and microscopic images of bilayer hydrogel for MSC osteochondrogenesis. (**i**) 3D stack image of confocal microscopy showing that MSCs preferentially underwent osteogenesis under DMS and chondrogenesis under static microenvironment. (**j,k**) The MSC differentiation preferences are represented by the intensity of secreted collagen type I and II in different hydrogel layers, which is related to osteogenesis and chondrogenesis, respectively. Data are expressed as mean ± SD, n = 4.

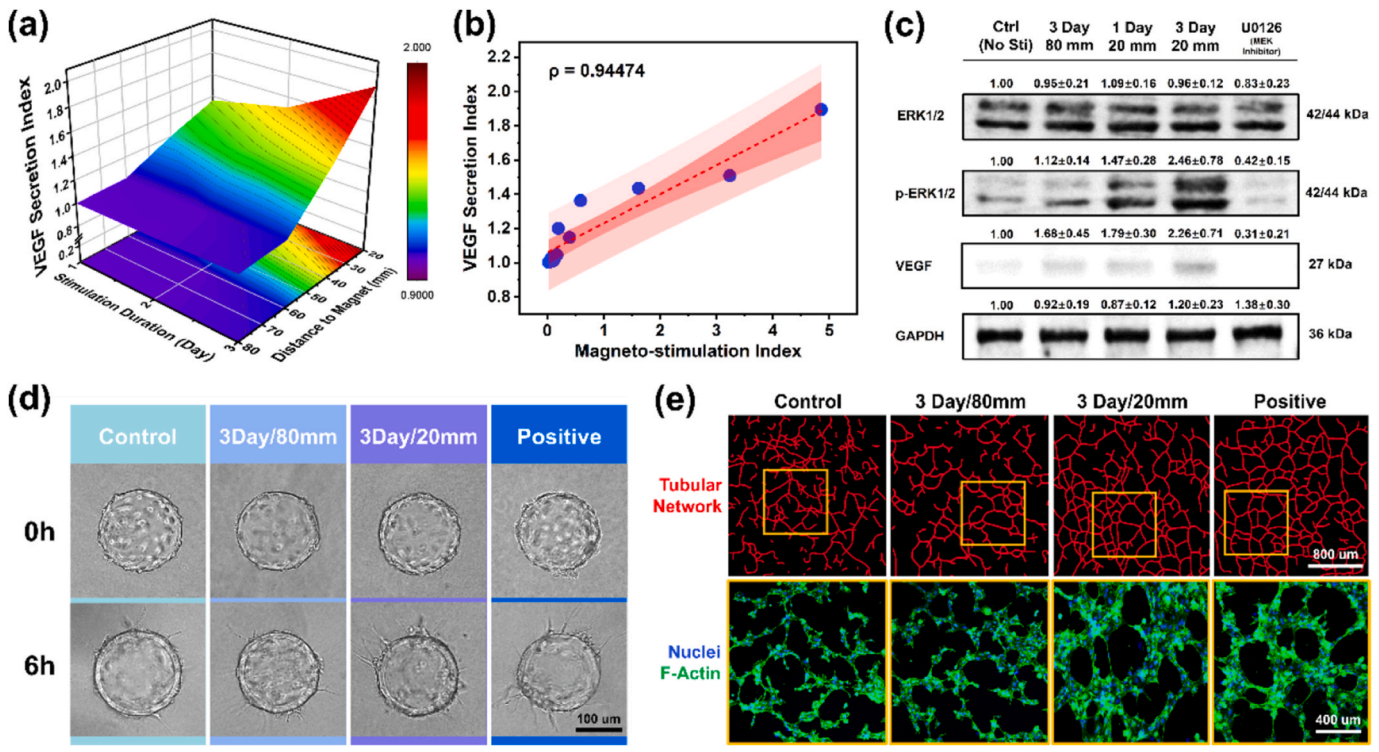

Fig. 6. Secretome of bone marrow-derived mesenchymal stem cells (MSCs) in GPM hydrogel. (**a**) Parametric analysis of MSC-derived vascular endothelial growth factor (VEGF) indicating that stronger and longer dynamic mechanical stimulation (DMS) favored VEGF production. (**b**) Strong positive correlation between VEGF secretion and external stimulation (ρ, Pearson coefficient). (**c**) Western blot analysis showing DMS promoted MSC VEGF secretion via *FAK-ERK* pathway. (**d**) Contrast brightfield images monitoring of angiogenic sprouting from fibrin gel beads in 0 and 6 h incubated in MSC conditioned medium under different culture conditions. (**e**) Tube formation bioassay of umbilical vein endothelial cells incubated with MSC conditioned medium from different culture conditions, showing that MSC conditioned medium under stronger DMS (i.e., 3Day/20 mm) had better angiogenic sprouting and vascularization network formation. Yellow frames represent the zone of below fluorescent images. Data are expressed as mean ± SD, n = 3.

formation (Fig. 6d,e and S32). VECs also had greater migration activity in '3Day/20 mm' medium which can be useful for vascular recruitment into bone defect (Fig. S33).

4. Discussion

MSC manufacturing and therapy is estimated to have achieved a revenue of USD ~3 billion in 2021 and is expected to expand at a compound annual growth rate of ~14% in the following years [90]. There is a need for better technologies to meet the manufacturing and clinical needs for the MSC therapy. Here, we developed a biomaterial-based strategy to boost MSC production and propose a direct route from MSC manufacturing to therapy with high cell viability. The ingredients of our hydrogel are biocompatible, with commercially available FDA-approved equivalent, making it easier to GMP compliance. We also combined DMS in our hydrogel for mechanical pre-conditioning to manufacture MSC [15,16] and to boost MSC proliferation rates.

Compared to large bioreactors, smaller manufacturing scale using 3D hydrogels is arguably more suitable for MSC therapies involving smaller cell numbers and localized delivery such as for joint regeneration and nasal bone repair/rhinoplasty [91,92], while offering potential for precision manufacturing over large-scale bioreactors. For MSC, it is crucial to maintain self-renewal and differentiation potential during cell expansion [10]. Harnessing the 3D environment and gentle dynamic stimulation in our GPM hydrogel, we found an improved MSC proliferation rate with negligible reduction in stemness to achieve a fine balance between cell quantity and quality in manufacturing. This is especially significant for autologous therapy where MSCs isolated from patients are few in numbers and highly heterogenous.

In addition, current MSC expansion protocols rely heavily on costly, animal-sourced serum, but as serum composition has significant batch-to-batch variation and may be contaminated with prions, viral and zoonotic agents [74,93], there has been tremendous interests to create chemically defined medium for MSC expansion or induce MSC to produce cytokines/growth factors during manufacturing [94]. In our GPM hydrogel, we observed enhanced MSC secretome including ~1.9-fold increase of VEGF and ~2.0-fold increase of bFGF under DMS, attributing to activation of mechanotransduction pathways. This may help reduce the use of animal-sourced serum and raw material costs. We believe that apart from these pro-angiogenesis growth factors, our DMS can influence other MSC paracrine productions to support MSC growth and expansion, and we plan to perform detailed proteomics studies with human MSCs in the future.

After generating sufficient cell numbers, for conventional bioreactor, MSCs are detached and separated from microcarriers by proteolytic enzyme, followed with washing and concentrating [95]. Likewise, in a 2D culture plates, MSCs have to be enzymatically treated and detached. However, these processing steps are known to damage/inactivate MSCs, particularly during cell detachment from substrate [96,97], and to avoid contamination, all steps must strictly comply with GMP requirements which is likely to result in high labor cost.

In GPM hydrogel, after *ex vivo* expansion, the cell-encapsulated hydrogel constructs can be used for therapy directly as an 'all-in-one' strategy from patient cell culture to manufacturing and final clinical use. This could help avoid potential issues including high-cost production, sophisticated downstream procedures, and cell damage from cell-substrate detachment. In addition, hydrogel material can protect cells to ensure high *in vivo* viability, whereas direct injection of cell solution may cause local leakage and ~50% cell death after transplantation [43]. Based on recent studies on the cryopreservation effect of hydrogel material, it will also be interesting to explore the potential of cryoprotective

effects of our GPM hydrogel which is another big challenge in MSC manufacturing [98].

Another big advantage of our dynamic 3D scaffold is that it can enhance the biofunctions of MSCs via wireless magnetic field. For example, for bone or cartilage repair, the scaffold complex can direct MSC osteo/chondrogenesis in differentiation-specific medium (i.e., biochemical stimuli), and further optimized through magneto-mechanical stimulation, to produce 'bone/cartilage tissue module'. Taking advantage of wireless magnetic control and deep tissue penetration, it is also possible to control MSC behaviors and their functions with the implanted GPM hydrogel *in vivo* to facilitate vascularization and osteogenesis in bone defect and enhance immunoregulation through MSC paracrine production. For the next step, after the *ex vivo* MSC manufacturing and functionalization in GPM hydrogel, we could study this 'all-in-one' functional hydrogel in animal models to assess its therapeutic effect, especially for bone repair due to enhanced MSC osteogenesis and pro-angiogenetic effects. Moreover, it is interesting to explore whether DMS can promote MSC growth and functionalization in GPM hydrogel *in vivo*. The cell-loaded hydrogel system could serve as a controllable implant that regulates cell behaviors through wireless DMS for tissue engineering.

5. Conclusions

In this study, we developed a 3D dynamic hydrogel using magneto-induced DMS to improve MSC manufacturing. Harnessing the 3D environment and gentle dynamic stimulation, in GPM hydrogel, we found an improved MSC proliferation rate with negligible reduction in MSC stemness, to optimize cell quantity and quality during manufacturing. Through enhancing matrix-integrin interactions and activating mechanotransduction pathways, we were also able to direct MSC differentiation and increased growth factor secretion by MSCs under DMS, which is critical for MSC therapy. More importantly, all these complex procedures, from MSC manufacturing to final clinical use, can be achieved in our hydrogel platform, making it an integrated solution from manufacturing to clinical use. Although more studies including longer cell expansion, GMP procedures, and post manufacturing quality analysis and control, are still needed, we believe this 'all-in-one' technology offers a novel paradigm shift to existing protocols in MSC therapy, particularly for applications requiring few but high-quality cells.

Credit author statement

Y·S., L.L., and Q.L. contribute equally to this work. Y.S., L.L., and A.T. conceived the ideas, designed the experiments, and analyzed the results. Y.S. performed all the experiments and analysis. L.L. was responsible of cell works, protein/gene characterizations, and animal works of MSCs. Q.L. and H.L. were responsible for magnetic force calculation and multiphysics modeling. Z.C. conducted cell feature characterization works. K.L.L. and C.C. conducted VEC experiment and characterization. X.L. conducted material fabrication and characterization. D.Z.K. contributed to polymer synthesis and material fabrication. Y.W. contributed to MSC works. C.T.L. contributed to material and cell immunofluorescent characterization. T.M.L., Z.Y., C.T.L., and C.C. contributed to manuscript writing. Y.S. and A.T. wrote and revised the manuscript. A.T. supervised the entire project. All authors critically read and revised the manuscript and approved its submission for publication. Refer to Table S2 for comprehensive breakdown of authors' contributions.

Ethics approval and consent to participate

Not applicable.

Declaration of competing interest

The authors declare that they have no known competing financial interests or personal relationships that could have appeared to influence the work reported in this paper.

Acknowledgements

The research was supported by NUS Presidential Young Professorship, MOE Tier 1 grant, and iHT OOE award. Y.S. is supported by the NUS Research Scholarship. Authors would like to appreciate technical assistance from Jonathan Yuin-Han Loh and Too Heng-Phon. Authors appreciate support from Shu Ying Lee and Xiaoning Wang (Confocal Microscopy Unit, NUS) in confocal imaging and flow cytometry usage and data analysis. Authors would like to acknowledge technical assistance from Suat Hoon Tan (Electron Microscopy Unit, NUS) for SEM and TEM usage. Scheme 1 and Figs. 1 and 5 are created with BioRender.com.

Appendix A. Supplementary data

Supplementary data to this article can be found online at https://doi.org/10.1016/j.bioactmat.2022.12.019.

References

[1] N. Kim, S.-G. Cho, Clinical applications of mesenchymal stem cells, Korean J. Intern. Med. 28 (2013) 387, https://doi.org/10.3904/kjim.2013.28.4.387.
[2] A. Musiał-Wysocka, M. Kot, M. Majka, The pros and cons of mesenchymal stem cell-based therapies, Cell Transplant. 28 (2019) 801–812, https://doi.org/10.1177/0963689719837897.
[3] S. Wang, X. Qu, R.C. Zhao, Clinical applications of mesenchymal stem cells, J. Hematol. Oncol. 5 (2012) 19, https://doi.org/10.1186/1756-8722-5-19.
[4] M.F. Pittenger, D.E. Discher, B.M. Péault, D.G. Phinney, J.M. Hare, A.I. Caplan, Mesenchymal stem cell perspective: cell biology to clinical progress, Npj Regen. Med. 4 (2019) 22, https://doi.org/10.1038/s41536-019-0083-6.
[5] F. Shang, Y. Yu, S. Liu, L. Ming, Y. Zhang, Z. Zhou, J. Zhao, Y. Jin, Advancing application of mesenchymal stem cell-based bone tissue regeneration, Bioact. Mater. 6 (2021) 666–683, https://doi.org/10.1016/j.bioactmat.2020.08.014.
[6] D.E. Rodríguez-Fuentes, L.E. Fernández-Garza, J.A. Samia-Meza, S.A. Barrera-Barrera, A.I. Caplan, H.A. Barrera-Saldaña, Mesenchymal stem cells current clinical applications: a systematic review, Arch. Med. Res. 52 (2021) 93–101, https://doi.org/10.1016/j.arcmed.2020.08.006.
[7] A. Wright, M.L. Arthaud-Day, M.L. Weiss, Therapeutic use of mesenchymal stromal cells: the need for inclusive characterization guidelines to accommodate all tissue sources and species, Front. Cell Dev. Biol. 9 (2021), 632717, https://doi.org/10.3389/fcell.2021.632717.
[8] A. Keating, Mesenchymal stromal cells, Curr. Opin. Hematol. 13 (2006) 419–425, https://doi.org/10.1097/01.moh.0000245697.54887.6f.
[9] Y.Y.F. Liu, Y. Lu, S. Oh, G.J. Conduit, Machine learning to predict mesenchymal stem cell efficacy for cartilage repair, PLoS Comput. Biol. 16 (2020), e1008275, https://doi.org/10.1371/journal.pcbi.1008275.
[10] D. Kouroupis, D. Correa, Increased mesenchymal stem cell functionalization in three-dimensional manufacturing settings for enhanced therapeutic applications, Front. Bioeng. Biotechnol. 9 (2021), 621748, https://doi.org/10.3389/fbioe.2021.621748.
[11] L. Yu, Y. Wu, J. Liu, B. Li, B. Ma, Y. Li, Z. Huang, Y. He, H. Wang, Z. Wu, G. Qiu, 3D culture of bone marrow-derived mesenchymal stem cells (BMSCs) could improve bone regeneration in 3D-printed porous Ti6Al4V scaffolds, 2018, Stem Cell. Int. (2018) 1–13, https://doi.org/10.1155/2018/2074021.
[12] M. Bicer, G.S. Cottrell, D. Widera, Impact of 3D cell culture on bone regeneration potential of mesenchymal stromal cells, Stem Cell Res. Ther. 12 (2021) 31, https://doi.org/10.1186/s13287-020-02094-8.
[13] Y. Shou, S.C. Johnson, Y.J. Quek, X. Li, A. Tay, Integrative lymph node-mimicking models created with biomaterials and computational tools to study the immune system, Mater, Today Biogr. 14 (2022), 100269, https://doi.org/10.1016/j.mtbio.2022.100269.
[14] X. Li, Y. Shou, A. Tay, Hydrogels for engineering the immune system, Adv. NanoBiomed Res. 1 (2021), 2000073, https://doi.org/10.1002/anbr.202000073.
[15] S. Davis, M. Roldo, G. Blunn, G. Tozzi, T. Roncada, Influence of the mechanical environment on the regeneration of osteochondral defects, Front. Bioeng. Biotechnol. 9 (2021), 603408, https://doi.org/10.3389/fbioe.2021.603408.
[16] K.H. Vining, D.J. Mooney, Mechanical forces direct stem cell behaviour in development and regeneration, Nat. Rev. Mol. Cell Biol. 18 (2017) 728–742, https://doi.org/10.1038/nrm.2017.108.
[17] R.C. Nordberg, G.A. Otarola, D. Wang, J.C. Hu, K.A. Athanasiou, Navigating regulatory pathways for translation of biologic cartilage repair products, Sci. Transl. Med. 14 (2022), https://doi.org/10.1126/scitranslmed.abp8163 eabp.8163.

[18] B.A. Aguado, W. Mulyasasmita, J. Su, K.J. Lampe, S.C. Heilshorn, Improving viability of stem cells during syringe needle flow through the Design of hydrogel cell carriers, Tissue Eng. 18 (2012) 806–815, https://doi.org/10.1089/ten.tea.2011.0391.
[19] Z.W. Wagoner, W. Zhao, Therapeutic implications of transplanted-cell death, Nat. Biomed. Eng. 5 (2021) 379–384, https://doi.org/10.1038/s41551-021-00729-6.
[20] D.J. Weiss, K. English, A. Krasnodembskaya, J.M. Isaza-Correa, I.J. Hawthorne, B. P. Mahon, The necrobiology of mesenchymal stromal cells affects therapeutic efficacy, Front. Immunol. 10 (2019), 01228, https://doi.org/10.3389/fimmu.2019.01228.
[21] A. Galleu, Y. Riffo-Vasquez, C. Trento, C. Lomas, L. Dolcetti, T.S. Cheung, M. von Bonin, L. Barbieri, K. Halai, S. Ward, L. Weng, R. Chakraverty, G. Lombardi, F. M. Watt, K. Orchard, D.I. Marks, J. Apperley, M. Bornhauser, H. Walczak, C. Bennett, F. Dazzi, Apoptosis in mesenchymal stromal cells induces in vivo recipient-mediated immunomodulation, Sci. Transl. Med. 9 (2017), https://doi.org/10.1126/scitranslmed.aam7828.
[22] F. Luk, S.F.H. de Witte, S.S. Korevaar, M. Roemeling-van Rhijn, M. Franquesa, T. Strini, S. van den Engel, M. Gargesha, D. Roy, F.J.M.F. Dor, E.M. Horwitz, R.W. F. de Bruin, M.G.H. Betjes, C.C. Baan, M.J. Hoogduijn, Inactivated mesenchymal stem cells maintain immunomodulatory capacity, Stem Cell. Dev. 25 (2016) 1342–1354, https://doi.org/10.1089/scd.2016.0068.
[23] J. Low, B. Chan, A. Tay, Targeted therapeutics delivery by exploiting biophysical properties of senescent cells, Adv. Funct. Mater. 32 (2022), 2107990, https://doi.org/10.1002/adfm.202107990.
[24] xiayi xu, Q. Feng, X. Ma, Y. Deng, K. Zhang, H.S. Ooi, B. Yang, Z.-Y. Zhang, B. Feng, L. Bian, Dynamic gelatin-based hydrogels promote the proliferation and self-renewal of embryonic stem cells in long-term 3D culture, Biomaterials 289 (2022), 121802, https://doi.org/10.1016/j.biomaterials.2022.121802.
[25] Y. Ren, H. Zhang, Y. Wang, B. Du, J. Yang, L. Liu, Q. Zhang, Hyaluronic acid hydrogel with adjustable stiffness for mesenchymal stem cell 3D culture via related molecular mechanisms to maintain stemness and induce cartilage differentiation, ACS Appl. Bio Mater. 4 (2021) 2601–2613, https://doi.org/10.1021/acsabm.0c01591.
[26] N.J. Steinmetz, E.A. Aisenbrey, K.K. Westbrook, H.J. Qi, S.J. Bryant, Mechanical loading regulates human MSC differentiation in a multi-layer hydrogel for osteochondral tissue engineering, Acta Biomater. 21 (2015) 142–153, https://doi.org/10.1016/j.actbio.2015.04.015.
[27] J.Y. Ng, K.Y.F. Tan, P.L.R. Ee, Sugar-assisted cryopreservation of stem cell-laden gellan gum–collagen interpenetrating network hydrogels, Biomacromolecules 23 (2022) 2803–2813, https://doi.org/10.1021/acs.biomac.2c00176.
[28] J.N. Roberts, J.K. Sahoo, L.E. McNamara, K.V. Burgess, J. Yang, E.V. Alakpa, H. J. Anderson, J. Hay, L.-A. Turner, S.J. Yarwood, M. Zelzer, R.O.C. Oreffo, R. V. Ulijn, M.J. Dalby, Dynamic surfaces for the study of mesenchymal stem cell growth through adhesion regulation, ACS Nano 10 (2016) 6667–6679, https://doi.org/10.1021/acsnano.6b01765.
[29] H.-H. Tsai, K.-C. Yang, M.-H. Wu, J.-C. Chen, C.-L. Tseng, The effects of different dynamic culture systems on cell proliferation and osteogenic differentiation in human mesenchymal stem cells, Int. J. Mol. Sci. 20 (2019) 4024, https://doi.org/10.3390/ijms20164024.
[30] H. Liu, J.F. Usprech, P.K. Parameshwar, Y. Sun, C.A. Simmons, Combinatorial screen of dynamic mechanical stimuli for predictive control of MSC mechano-responsiveness, Sci. Adv. 7 (2021), https://doi.org/10.1126/sciadv.abe7204 eabe7204.
[31] C. Moraes, Y. Sun, C.A. Simmons, (Micro)managing the mechanical microenvironment, Integr. Biol. 3 (2011) 959, https://doi.org/10.1039/c1ib00056j.
[32] L. MacQueen, Y. Sun, C.A. Simmons, Mesenchymal stem cell mechanobiology and emerging experimental platforms, J. R. Soc. Interface 10 (2013), https://doi.org/10.1098/rsif.2013.0179, 20130179.
[33] C.M. Bidan, M. Fratzl, A. Coullomb, P. Moreau, A.H. Lombard, I. Wang, M. Balland, T. Boudou, N.M. Dempsey, T. Devillers, A. Dupont, Magneto-active substrates for local mechanical stimulation of living cells, Sci. Rep. 8 (2018) 1464, https://doi.org/10.1038/s41598-018-19804-1.
[34] A. Cochis, S. Grad, M.J. Stoddart, S. Farè, L. Altomare, B. Azzimonti, M. Alini, L. Rimondini, Bioreactor mechanically guided 3D mesenchymal stem cell chondrogenesis using a biocompatible novel thermo-reversible methylcellulose-based hydrogel, Sci. Rep. 7 (2017), 45018, https://doi.org/10.1038/srep45018.
[35] S. Lin, W.Y.W. Lee, Q. Feng, L. Xu, B. Wang, G.C.W. Man, Y. Chen, X. Jiang, L. Bian, L. Cui, B. Wei, G. Li, Synergistic effects on mesenchymal stem cell-based cartilage regeneration by chondrogenic preconditioning and mechanical stimulation, Stem Cell Res. Ther. 8 (2017) 221, https://doi.org/10.1186/s13287-017-0672-5.
[36] C. Liu, Q. Yu, Z. Yuan, Q. Guo, X. Liao, F. Han, T. Feng, G. Liu, R. Zhao, Z. Zhu, H. Mao, C. Zhu, B. Li, Engineering the viscoelasticity of gelatin methacryloyl (GelMA) hydrogels via small "dynamic bridges" to regulate BMSC behaviors for osteochondral regeneration, Bioact. Mater. (2022), https://doi.org/10.1016/j.bioactmat.2022.07.031.
[37] Z. Tong, L. Jin, J.M. Oliveira, R.L. Reis, Q. Zhong, Z. Mao, C. Gao, Adaptable hydrogel with reversible linkages for regenerative medicine: dynamic mechanical microenvironment for cells, Bioact. Mater. 6 (2021) 1375–1387, https://doi.org/10.1016/j.bioactmat.2020.10.029.
[38] I. Pepelanova, K. Kruppa, T. Scheper, A. Lavrentieva, Gelatin-methacryloyl (GelMA) hydrogels with defined degree of functionalization as a versatile toolkit for 3D cell culture and extrusion bioprinting, Bioengineering 5 (2018) 55, https://doi.org/10.3390/bioengineering5030055.
[39] H. Shirahama, B.H. Lee, L.P. Tan, N.-J. Cho, Precise tuning of facile one-pot gelatin methacryloyl (GelMA) synthesis, Sci. Rep. 6 (2016), 31036, https://doi.org/10.1038/srep31036.
[40] L. Gu, T. Li, X. Song, X. Yang, S. Li, L. Chen, P. Liu, X. Gong, C. Chen, L. Sun, Preparation and characterization of methacrylated gelatin/bacterial cellulose composite hydrogels for cartilage tissue engineering, Regen. Biomater. 7 (2020) 195–202, https://doi.org/10.1093/rb/rbz050.
[41] M. Zhu, Y. Wang, G. Ferracci, J. Zheng, N.-J. Cho, B.H. Lee, Gelatin methacryloyl and its hydrogels with an exceptional degree of controllability and batch-to-batch consistency, Sci. Rep. 9 (2019) 6863, https://doi.org/10.1038/s41598-019-42186-x.
[42] S. Krishnamoorthy, B. Noorani, C. Xu, Effects of encapsulated cells on the physical–mechanical properties and microstructure of gelatin methacrylate hydrogels, Int. J. Mol. Sci. 20 (2019) 5061, https://doi.org/10.3390/ijms20205061.
[43] Z. Shi, Q. Wang, G.-F. Li, Y.-F. Shou, H.-J. Zong, S.-F. Yan, K.-X. Zhang, J.-B. Yin, Preparation and characterization of attractive poly(amino acid) hydrogels based on 2-ureido-4[1H]-pyrimidinone, Chin. J. Polym. Sci. 39 (2021) 327–336, https://doi.org/10.1007/s10118-021-2498-y.
[44] Y. Shou, S.B. Campbell, A. Lam, A.J. Lausch, J.P. Santerre, M. Radisic, L. Davenport Huyer, Toward renewable and functional biomedical polymers with tunable degradation rates based on itaconic acid and 1,8-octanediol, ACS Appl. Polym. Mater. 3 (2021) 1943–1955, https://doi.org/10.1021/acsapm.1c00017.
[45] K. Chatterjee, S. Lin-Gibson, W.E. Wallace, S.H. Parekh, Y.J. Lee, M.T. Cicerone, M. F. Young, C.G. Simon, The effect of 3D hydrogel scaffold modulus on osteoblast differentiation and mineralization revealed by combinatorial screening, Biomaterials 31 (2010) 5051–5062, https://doi.org/10.1016/j.biomaterials.2010.03.024.
[46] J. Chen, Z.-D. Shi, X. Ji, J. Morales, J. Zhang, N. Kaur, S. Wang, Enhanced osteogenesis of human mesenchymal stem cells by periodic heat shock in self-assembling peptide hydrogel, Tissue Eng. 19 (2013) 716–728, https://doi.org/10.1089/ten.tea.2012.0070.
[47] H. Yang, N.M.J. Cheam, H. Cao, M.K.H. Lee, S.K. Sze, N.S. Tan, C.Y. Tay, Materials stiffness-dependent redox metabolic reprogramming of mesenchymal stem cells for secretome-based therapeutic angiogenesis, Adv. Healthc. Mater. 8 (2019), 1900929, https://doi.org/10.1002/adhm.201900929.
[48] M.N. Nakatsu, J. Davis, C.C.W. Hughes, Optimized fibrin gel bead assay for the study of angiogenesis, JoVE (2007) 186, https://doi.org/10.3791/186.
[49] N. Davidenko, C.F. Schuster, D.V. Bax, R.W. Farndale, S. Hamaia, S.M. Best, R. E. Cameron, Correction to: evaluation of cell binding to collagen and gelatin: a study of the effect of 2D and 3D architecture and surface chemistry, J. Mater. Sci. Mater. Med. 27 (2018) 39, https://doi.org/10.1007/s10856-018-6047-3.
[50] S.L. Bellis, Advantages of RGD peptides for directing cell association with biomaterials, Biomaterials 32 (2011) 4205–4210, https://doi.org/10.1016/j.biomaterials.2011.02.029.
[51] A. Cavallo, M. Madaghiele, U. Masullo, M.G. Lionetto, A. Sannino, Photo-crosslinked poly(ethylene glycol) diacrylate (PEGDA) hydrogels from low molecular weight prepolymer: swelling and permeation studies, J. Appl. Polym. Sci. 134 (2017), 44380, https://doi.org/10.1002/app.44380.
[52] B. Oktay, S. Demir, N. Kayaman-Apohan, Magnetic nanoparticle containing thiol-ene crosslinked hydrogels for controlled and targeted release of hydrophobic drugs, Polym. Compos. 39 (2018) E200, https://doi.org/10.1002/pc.24144. –E209.
[53] R. Nagarjuna, M.S.M. Saifullah, R. Ganesan, Oxygen insensitive thiol–ene photo-click chemistry for direct imprint lithography of oxides, RSC Adv. 8 (2018) 11403–11411, https://doi.org/10.1039/C8RA01688G.
[54] H. Du, G. Zha, L. Gao, H. Wang, X. Li, Z. Shen, W. Zhu, Fully biodegradable antibacterial hydrogels via thiol–ene "click" chemistry, Polym. Chem. 5 (2014) 4002–4008, https://doi.org/10.1039/C4PY00030G.
[55] A. Tay, A. Kunze, D. Jun, E. Hoek, D. Di Carlo, The age of cortical neural networks affects their interactions with magnetic nanoparticles, Small 12 (2016) 3559–3567, https://doi.org/10.1002/smll.201600673.
[56] N. Lewinski, V. Colvin, R. Drezek, Cytotoxicity of nanoparticles, Small 4 (2008) 26–49, https://doi.org/10.1002/smll.200700595.
[57] K.M. Schultz, K.A. Kyburz, K.S. Anseth, Measuring dynamic cell–material interactions and remodeling during 3D human mesenchymal stem cell migration in hydrogels, Proc. Natl. Acad. Sci. USA 112 (2015) E3757–E3764, https://doi.org/10.1073/pnas.1511304112.
[58] R. Messing, N. Frickel, L. Belkoura, R. Strey, H. Rahn, S. Odenbach, A.M. Schmidt, Cobalt ferrite nanoparticles as multifunctional cross-linkers in PAAm ferrohydrogels, Macromolecules 44 (2011) 2990–2999, https://doi.org/10.1021/ma102708b.
[59] A. Simon-Deckers, S. Loo, M. Mayne-L'hermite, N. Herlin-Boime, N. Menguy, C. Reynaud, B. Gouget, M. Carrière, Size-, composition- and shape-dependent toxicological impact of metal oxide nanoparticles and carbon nanotubes toward bacteria, Environ. Sci. Technol. 43 (2009) 8423–8429, https://doi.org/10.1021/es9016975.
[60] M. Tarantola, A. Pietuch, D. Schneider, J. Rother, E. Sunnick, C. Rosman, S. Pierrat, C. Sönnichsen, J. Wegener, A. Janshoff, Toxicity of gold-nanoparticles: synergistic effects of shape and surface functionalization on micromotility of epithelial cells, Nanotoxicology 5 (2011) 254–268, https://doi.org/10.3109/17435390.2010.528847.
[61] W. Chen, Y. Zhang, J. Kumari, H. Engelkamp, P.H.J. Kouwer, Magnetic stiffening in 3D cell culture matrices, Nano Lett. 21 (2021) 6740–6747, https://doi.org/10.1021/acs.nanolett.1c00371.
[62] S. Massou, F. Nunes Vicente, F. Wetzel, A. Mehidi, D. Strehle, C. Leduc, R. Voituriez, O. Rossier, P. Nassoy, G. Giannone, Cell stretching is amplified by

active actin remodelling to deform and recruit proteins in mechanosensitive structures, Nat. Cell Biol. 22 (2020) 1011–1023, https://doi.org/10.1038/s41556-020-0548-2.
[63] S. Kakinoki, J.-H. Seo, Y. Inoue, K. Ishihara, N. Yui, T. Yamaoka, Mobility of the Arg-Gly-Asp ligand on the outermost surface of biomaterials suppresses integrin-mediated mechanotransduction and subsequent cell functions, Acta Biomater. 13 (2015) 42–51, https://doi.org/10.1016/j.actbio.2014.11.020.
[64] T. Yan, D. Rao, Y. Chen, Y. Wang, Q. Zhang, S. Wu, Magnetic nanocomposite hydrogel with tunable stiffness for probing cellular responses to matrix stiffening, Acta Biomater. 138 (2022) 112–123, https://doi.org/10.1016/j.actbio.2021.11.001.
[65] D.S.H. Wong, J. Li, X. Yan, B. Wang, R. Li, L. Zhang, L. Bian, Magnetically tuning tether mobility of integrin ligand regulates adhesion, spreading, and differentiation of stem cells, Nano Lett. 17 (2017) 1685–1695, https://doi.org/10.1021/acs.nanolett.6b04958.
[66] Y. Yang, T. Xu, H.-P. Bei, L. Zhang, C.-Y. Tang, M. Zhang, C. Xu, L. Bian, K.W.-K. Yeung, J.Y.H. Fuh, X. Zhao, Gaussian curvature–driven direction of cell fate toward osteogenesis with triply periodic minimal surface scaffolds, Proc. Natl. Acad. Sci. USA 119 (2022), https://doi.org/10.1073/pnas.2206684119.
[67] H. Kang, S. Kim, D.S.H. Wong, H.J. Jung, S. Lin, K. Zou, R. Li, G. Li, V.P. Dravid, L. Bian, Remote manipulation of ligand nano-oscillations regulates adhesion and polarization of macrophages in vivo, Nano Lett. 17 (2017) 6415–6427, https://doi.org/10.1021/acs.nanolett.7b03405.
[68] R.O. Hynes, Integrins: bidirectional, allosteric signaling machines, Cell 110 (2002) 673–687, https://doi.org/10.1016/S0092-8674(02)00971-6.
[69] M.M. Riopel, J. Li, S. Liu, A. Leask, R. Wang, β1 integrin–extracellular matrix interactions are essential for maintaining exocrine pancreas architecture and function, Lab. Invest. 93 (2013) 31–40, https://doi.org/10.1038/labinvest.2012.147.
[70] D. Zwolanek, M. Flicker, E. Kirstätter, F. Zaucke, G.J.V.M. van Osch, R.G. Erben, β1 integrins mediate attachment of mesenchymal stem cells to cartilage lesions, BioResearch Open Access 4 (2015) 39–53, https://doi.org/10.1089/biores.2014.0055.
[71] A.-R. Qian, X. Gao, W. Zhang, J.-B. Li, Y. Wang, S.-M. Di, L.-F. Hu, P. Shang, Large gradient high magnetic fields affect osteoblast ultrastructure and function by disrupting collagen I or fibronectin/αβ1 integrin, PLoS One 8 (2013), e51036, https://doi.org/10.1371/journal.pone.0051036.
[72] S. Di, Z. Tian, A. Qian, J. Li, J. Wu, Z. Wang, D. Zhang, D. Yin, M.L. Brandi, P. Shang, Large gradient high magnetic field affects FLG29.1 cells differentiation to form osteoclast-like cells, Int. J. Radiat. Biol. 88 (2012) 806–813, https://doi.org/10.3109/09553002.2012.698365.
[73] C.J.K. Wong, Y.K. Tai, J.L.Y. Yap, C.H.H. Fong, L.S.W. Loo, M. Kukumberg, J. Fröhlich, S. Zhang, J.Z. Li, J.-W. Wang, A.J. Rufaihah, A. Franco-Obregón, Brief exposure to directionally-specific pulsed electromagnetic fields stimulates extracellular vesicle release and is antagonized by streptomycin: a potential regenerative medicine and food industry paradigm, Biomaterials 287 (2022), 121658, https://doi.org/10.1016/j.biomaterials.2022.121658.
[74] N.D. Kadir, Z. Yang, A. Hassan, V. Denslin, E.H. Lee, Electrospun fibers enhanced the paracrine signaling of mesenchymal stem cells for cartilage regeneration, Stem Cell Res. Ther. 12 (2021) 100, https://doi.org/10.1186/s13287-021-02137-8.
[75] J.-M. Kim, Y.-S. Yang, K.H. Park, H. Oh, M.B. Greenblatt, J.-H. Shim, The ERK MAPK pathway is essential for skeletal development and homeostasis, Int. J. Mol. Sci. 20 (2019) 1803, https://doi.org/10.3390/ijms20081803.
[76] Y. Yang, X. Wang, Y. Wang, X. Hu, N. Kawazoe, Y. Yang, G. Chen, Influence of cell spreading area on the osteogenic commitment and phenotype maintenance of mesenchymal stem cells, Sci. Rep. 9 (2019) 6891, https://doi.org/10.1038/s41598-019-43362-9.
[77] S. Kaonis, Z. Aboellail, S. Ghosh, Characterization of mechanics driven heterogeneity in mesenchymal stromal cells, bioRxiv (2022), https://doi.org/10.1101/2022.07.25.501486.
[78] S.-M. Han, S.-H. Han, Y.-R. Coh, G. Jang, J. Chan Ra, S.-K. Kang, H.-W. Lee, H.-Y. Youn, Enhanced proliferation and differentiation of Oct4- and Sox2-overexpressing human adipose tissue mesenchymal stem cells, Exp. Mol. Med. 46 (2014), https://doi.org/10.1038/emm.2014.28 e101–e101.
[79] M.N. Knight, K.D. Hankenson, Mesenchymal stem cells in bone regeneration, Adv. Wound Care 2 (2013) 306–316, https://doi.org/10.1089/wound.2012.0420.
[80] C. Popov, M. Burggraf, L. Kreja, A. Ignatius, M. Schieker, D. Docheva, Mechanical stimulation of human tendon stem/progenitor cells results in upregulation of matrix proteins, integrins and MMPs, and activation of p38 and ERK1/2 kinases, BMC Mol. Biol. 16 (2015) 6, https://doi.org/10.1186/s12867-015-0036-6.
[81] D. Wang, C.C.M. Pun, S. Huang, T.C.M. Tang, K.K.W. Ho, B.B. Rothrauff, P.S. H. Yung, A.M. Blocki, E.D.F. Ker, R.S. Tuan, Tendon-derived extracellular matrix induces mesenchymal stem cell tenogenesis via an integrin/transforming growth factor-β crosstalk-mediated mechanism, Faseb. J. 34 (2020) 8172–8186, https://doi.org/10.1096/fj.201902377RR.
[82] K.A. Kilian, B. Bugarija, B.T. Lahn, M. Mrksich, Geometric cues for directing the differentiation of mesenchymal stem cells, Proc. Natl. Acad. Sci. USA 107 (2010) 4872–4877, https://doi.org/10.1073/pnas.0903269107.
[83] P.S. Mathieu, E.G. Loboa, Cytoskeletal and focal adhesion influences on mesenchymal stem cell shape, mechanical properties, and differentiation down osteogenic, adipogenic, and chondrogenic pathways, Tissue Eng. B Rev. 18 (2012) 436–444, https://doi.org/10.1089/ten.teb.2012.0014.
[84] C. Gegg, F. Yang, The effects of ROCK inhibition on mesenchymal stem cell chondrogenesis are culture model dependent, Tissue Eng. 26 (2020) 130–139, https://doi.org/10.1089/ten.tea.2019.0068.
[85] R. McBeath, D.M. Pirone, C.M. Nelson, K. Bhadriraju, C.S. Chen, Cell shape, cytoskeletal tension, and RhoA regulate stem cell lineage commitment, Dev. Cell 6 (2004) 483–495, https://doi.org/10.1016/S1534-5807(04)00075-9.
[86] X. Liang, P. Duan, J. Gao, R. Guo, Z. Qu, X. Li, Y. He, H. Yao, J. Ding, Bilayered PLGA/PLGA-HAp composite scaffold for osteochondral tissue engineering and tissue regeneration, ACS Biomater. Sci. Eng. 4 (2018) 3506–3521, https://doi.org/10.1021/acsbiomaterials.8b00552.
[87] T.J. Levingstone, C. Moran, H.V. Almeida, D.J. Kelly, F.J. O'Brien, Layer-specific stem cell differentiation in tri-layered tissue engineering biomaterials: towards development of a single-stage cell-based approach for osteochondral defect repair, Mater. Today Bio. 12 (2021), 100173, https://doi.org/10.1016/j.mtbio.2021.100173.
[88] G. Kasper, N. Dankert, J. Tuischer, M. Hoeft, T. Gaber, J.D. Glaeser, D. Zander, M. Tschirschmann, M. Thompson, G. Matziolis, G.N. Duda, Mesenchymal stem cells regulate angiogenesis according to their mechanical environment, Stem Cell. 25 (2007) 903–910, https://doi.org/10.1634/stemcells.2006-0432.
[89] Y. Sun, B. Wan, R. Wang, B. Zhang, P. Luo, D. Wang, J.-J. Nie, D. Chen, X. Wu, Mechanical stimulation on mesenchymal stem cells and surrounding microenvironments in bone regeneration: regulations and applications, Front. Cell Dev. Biol. 10 (2022), 808303, https://doi.org/10.3389/fcell.2022.808303.
[90] Kenneth Research, Global mesenchymal stem cell (MSC) market. https://www.kennethresearch.com/report-details/mesenchymal-stem-cells-market/10082369, 2022.
[91] H. Le, W. Xu, X. Zhuang, F. Chang, Y. Wang, J. Ding, Mesenchymal stem cells for cartilage regeneration, J. Tissue Eng. 11 (2020), 204173142094383, https://doi.org/10.1177/2041731420943839.
[92] M. Wagenbrenner, S. Mayer-Wagner, M. Rudert, B.M. Holzapfel, M. Weissenberger, Combinations of hydrogels and mesenchymal stromal cells (MSCs) for cartilage tissue engineering—a review of the literature, Gels 7 (2021) 217, https://doi.org/10.3390/gels7040217.
[93] K.M. Panchalingam, S. Jung, L. Rosenberg, L.A. Behie, Bioprocessing strategies for the large-scale production of human mesenchymal stem cells: a review, Stem Cell Res. Ther. 6 (2015) 225, https://doi.org/10.1186/s13287-015-0228-5.
[94] A. Oikonomopoulos, W.K. van Deen, A.-R. Manansala, P.N. Lacey, T.A. Tomakili, A. Ziman, D.W. Hommes, Optimization of human mesenchymal stem cell manufacturing: the effects of animal/xeno-free media, Sci. Rep. 5 (2015), 16570, https://doi.org/10.1038/srep16570.
[95] V. Jossen, C. van den Bos, R. Eibl, D. Eibl, Manufacturing human mesenchymal stem cells at clinical scale: process and regulatory challenges, Appl. Microbiol. Biotechnol. 102 (2018) 3981–3994, https://doi.org/10.1007/s00253-018-8912-x.
[96] K. Tsuji, M. Ojima, K. Otabe, M. Horie, H. Koga, I. Sekiya, T. Muneta, Effects of different cell-detaching methods on the viability and cell surface antigen expression of synovial mesenchymal stem cells, Cell Transplant. 26 (2017) 1089–1102, https://doi.org/10.3727/096368917X694831.
[97] Y. Kurashina, C. Imashiro, M. Hirano, T. Kuribara, K. Totani, K. Ohnuma, J. Friend, K. Takemura, Enzyme-free release of adhered cells from standard culture dishes using intermittent ultrasonic traveling waves, Commun. Biol. 2 (2019) 393, https://doi.org/10.1038/s42003-019-0638-5.
[98] D. García-Bernal, M. García-Arranz, R.M. Yáñez, R. Hervás-Salcedo, A. Cortés, M. Fernández-García, M. Hernando-Rodríguez, Ó. Quintana-Bustamante, J. A. Bueren, D. García-Olmo, J.M. Moraleda, J.C. Segovia, A.G. Zapata, The current status of mesenchymal stromal cells: controversies, unresolved issues and some promising solutions to improve their therapeutic efficacy, Front. Cell Dev. Biol. 9 (2021), 650664, https://doi.org/10.3389/fcell.2021.650664.